University of Nevada, Reno

Direct Power Control of AC Motors

A thesis submitted in partial fulfillment of the
requirements for the degree of Master of Science in
Electrical Engineering

By

Xiaozhong Luo
Dr. Andrzej M. Trzynadlowski /Thesis Advisor

December, 2009

UNIVERSITY
OF NEVADA
RENO

THE GRADUATE SCHOOL

We recommend that the thesis

prepared under our supervision by

XIAOZHONG LUO

entitled

Direct Power Control of AC Motors

be accepted in partial fulfillment of the

requirements for the degree of

MASTER OF SCIENCE

Andrzej M. Trzynadlowski, Ph, D., Advisor

Cristian Lascu, Ph. D., Committee Member

Krishnan S. Raja, Ph. D., Graduate School Representative

Marsha H. Read, Ph. D., Associate Dean, Graduate School

December, 2009

ABSTRACT

In this thesis, the possibilities of direct power control (DPC) of induction motors (IMs) and permanent magnet synchronous motors (PMSMs) fed by a voltage source inverter have been studied. Three different approaches of DPC for IMs and one for PMSMs are proposed and investigated. They are: (a) direct output power and flux control, direct input power and flux control, and direct real power and reactive power control for IMs and (b) direct real and reactive power control for PMSMs. Principles of these approaches have been separately derived and evaluated. The reference values of control variables are discussed, and estimation of the actual values of those variables is provided. Simulation programs were written for the closed-loop speed control systems under various load conditions to verify the proposed methods.

Results of this study show that DPC of IMs works well with the output power and flux control, somewhat worse with the input power and flux control, but not so well with the real and reactive power control. It is hoped the investigation will facilitate further studies of DPC of IMs. The best result of this research is the successful direct power control of PMSMs.

Keywords: DPC, direct power control, direct power and flux control, induction motor, IM, permanent magnet synchronous motor, PMSM, real power, reactive power, voltage source inverter, hysteresis control.

ACKNOWLEDGEMENT

First of all, I would like to thank my advisor, Dr. Andrzej M. Trzynadlowski, for his patience, continuous help and support during my research work of this thesis. I switched to the motor control and electric drive area in the middle of my graduate study. Dr. Trzynadlowski walked me through basic to advanced topics in this field, and has guided me to the right direction and given me great advices in my study. I am very grateful to have a chance working with such a knowledgeable professor and a nice gentleman.

I would also like to thank Dr. Cristian Lascu, not only for his valuable detailed suggestions during my research to which this thesis relates, but also for his help and sharing knowledge and experience with me in other lab works as well.

I also want to express my gratitude to Dr. Krishnan S. Raja, for accepting my request from a busy schedule without hesitation to be a member of my graduate study committee.

Finally, I want to thank my family for supporting me all the way through my graduate study and my research. It would be much harder for me without their support.

TABLE OF CONTENTS

LIST OF TABLES

LIST OF FIGURES

LIST OF SYMBOLS

R_s	Stator resistance
R_r	Rotor resistance
L_s	Stator inductance
L_r	Rotor inductance
L_m	Magnetizing inductance
L_{ls}	Stator leakage inductance
L_{lr}	Rotor leakage inductance
ω_s	Stator electrical angular speed
ω_r	Rotor electrical angular speed
ω_{sl}	Electrical angular slip speed
ω_m	Mechanical angular speed
s	Slip
θ_s	Stator flux angle
θ_r	Rotor flux angle
p	Number of motor pole pairs
T_e	Electromagnetic torque
T_{ld}	Load torque
λ_s	Stator flux linkage

λ_r	Rotor flux linkage
λ_f	Permanent magnet flux linkage
V_{dc}	DC link voltage
v_s	Stator voltage
i_s	Stator current
J_L	Load mass moment of inertia
J_M	Rotor mass moment of inertia
P_{in}	Input real power
P_e	Electromagnetic power
P_m	Mechanical output power
P_{out}	Output real power

CHAPTER I

INTRODUCTION

AC motors are the most widely used electrical machines because of their inexpensiveness, robustness, and low maintenance costs. The most common AC motors are the induction motors (IMs), permanent-magnet synchronous motors (PMSMs), and the so-called brushless DC motors (BLDCs), which in fact are close relatives of PMSMs. The IMs have a long history of widespread industrial applications, but the PMSMs and BDCMs become increasingly popular in adjustable-speed drives thanks to the rapid progress in technology of high-energy permanent magnets. The IMs and PMSMs are the subject of this study.

In order to control an AC motor, a DC-AC converter, also known as an inverter, is employed. It is usually controlled using a digital signal processor (DSP) or a microcontroller. Figure 1.1 shows a typical AC drive system. In certain applications such as electric cars, the rectifier and the grid are replaced with a battery.

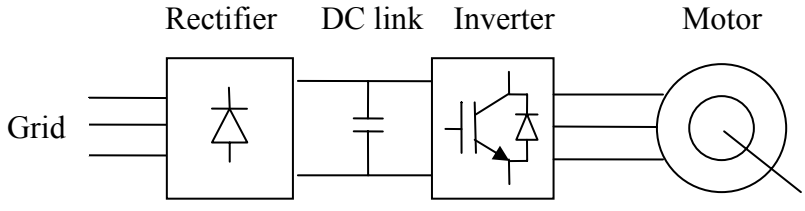

Figure 1.1 Block diagram of a typical AC drive system.

1.1 Control Techniques of AC Motors

Control of the AC motors can be done using various techniques. Most common techniques are: (a) constant voltage/frequency control (V/FC), (b) field orientation control (FOC), and (c) direct torque control (DTC). The first one is considered as scalar control since it adjusts only magnitude and frequency of the voltage or current with no concern about the instantaneous values of motor quantities. It does not require knowledge of parameters of the motor, and it is an open-loop control. Thus, it is a low cost simple solution for low-performance applications such as fans and pumps. The other two methods are in the space vector control category because they utilize both magnitude and angular position of space vectors of motor variables, such as the voltage and flux. They are employed in high performance applications, such as positioning drives or electric vehicles.

With the V/FC and FOC dominating the market now, DTC is gaining share in IM control, while still actively researched. The DTC for PMSMs has not been yet seen in commercial drives.

1.2 Research on Power Control of Electric Machines

Power control in electric machines has been a research topic since as early as 1990s. However, publications about direct power control (DPC) are only aimed at either rectifiers or generators, and not at IMs or PMSMs. Paper [1] is about a DPC of 3-phase synchronous rectifier. In [2], direct real power and reactive power control is applied to an

induction generator for wind energy systems. Publication [3] describes DPC in a power converter for improving the power factor. Paper [4] proposes DPC to rectifiers using the virtual flux. Reactive power compensation is discussed in [5]. What is in common among these applications is that they all are power output devices needed to provide real power to the load. However, in IMs or PMSMs fed by inverters, the controlled variable is the torque, because we want to control the position or speed, which are directly related to the torque applied.

The real power is related to the torque and imaginary power to the magnetic flux, and it is the power and energy that are consumed or generated in an electric motor. This is the idea behind the proposed power control of IMs. Research papers [6] and [7] present successful instantaneous power control of IMs. However, current control is involved inside the power control loop. Therefore this technique cannot be considered as direct power control, being conceptually closer to FOC. Control methods that are motor parameter dependent result in complexity of the control. The parameter estimation errors when the parameters change cause deterioration of motor operation.

1.3 Research Objective

In DTC of IMs and PMSMs, the actual control variable torque is very difficult to measure in practice. The feedback applied to the torque controller is exclusively estimated through algorithms thus is vulnerable to many factors such as model accuracy, parameter change etc. In DPC, both actual real power and reactive power as feedbacks for the controllers can be easily measured through voltage and current in a real system, reflecting the real actual values of the control variables.

The research presented in this thesis is devoted to the possibility of DPC of IMs and PMSMs that would be similar to the DTC, with the accompanying simplicity of implementation and independence of motor parameters.

1.4 Structure of the Thesis

This thesis is organized as follows. Chapter I is the introduction, while Chapter II provides background knowledge about AC motor control used in this study. The power flow and its simplification in the IM and PMSMs are described in Chapter III. A review of principles of the direct toque control (DTC) of IMs is provided in Chapter IV. Afterwards, three different approaches of direct power control of IMs are examined in terms of control principles and implementation issues, in Chapter V, VI and VII respectively. Simulation results of the first two methods are included in the same chapter. Finally, in Chapter VIII, the principles of DPC of PMSMs are derived as well as the implementation equations, and the simulation results are presented. Chapter IX concludes the thesis.

CHAPTER II

BACKGROUND

The background knowledge in motor control and power electronics that will be needed for the analysis and simulations presented in this thesis is explained briefly in this chapter. That includes the concepts of voltage space vectors and voltage source inverter, mathematical models of IMs and PMSMs, etc.

2.1 Voltage Space Vector

For the balanced three-phase system voltages, the voltage vector is defined as

$$\vec{v} = \vec{v}_a + \vec{v}_b + \vec{v}_c = v_a + v_b e^{j\frac{2\pi}{3}} + v_c e^{j\frac{4\pi}{3}} \tag{2.1}$$

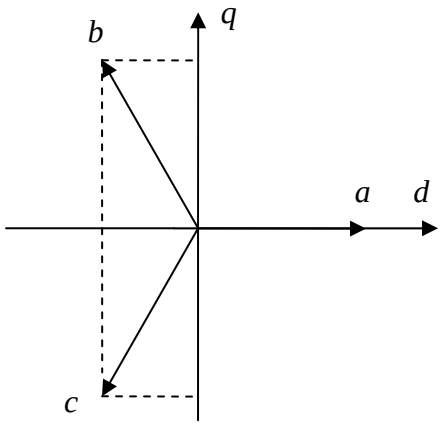

Figure 2.1 Transformation from 3-phase a-b-c system to 2-phase d-q system.

When describing the three-phase system with a more compact two phase stationary system, we have $\vec{v} = v_d + jv_q$ in d-q plane where the imaginary q axis is 90º ahead of the real d axis, as seen in Figure 2.1.

The transformation from a 3-phase a-b-c system to the 2-phase d-q stationary system is easy when the d-axis is aligned with the a-axis as shown in Figure 2.1, thus

$$v_d = v_a - \frac{1}{2}v_b - \frac{1}{2}v_c \tag{2.2}$$

$$v_q = \frac{\sqrt{3}}{2}v_b - \frac{\sqrt{3}}{2}v_c \tag{2.3}$$

that is,

$$\begin{bmatrix} v_d \\ v_q \end{bmatrix} = \begin{bmatrix} 1 & -\frac{1}{2} & -\frac{1}{2} \\ 0 & \frac{\sqrt{3}}{2} & -\frac{\sqrt{3}}{2} \end{bmatrix} \begin{bmatrix} v_a \\ v_b \\ v_c \end{bmatrix} \tag{2.4}$$

Considering a balanced system $v_a + v_b + v_c = 0$, the inverse transformation is

$$\begin{bmatrix} v_a \\ v_b \\ v_c \end{bmatrix} = \begin{bmatrix} \frac{2}{3} & 0 \\ -\frac{1}{3} & \frac{1}{\sqrt{3}} \\ -\frac{1}{3} & -\frac{1}{\sqrt{3}} \end{bmatrix} \begin{bmatrix} v_d \\ v_q \end{bmatrix} \tag{2.5}$$

The same conversions apply to currents.

Figure 2.2 illustrates the space vectors of the most commonly used two level voltage source inverters. Vector $\vec{v}_1$ to $\vec{v}_6$ are the six real voltage vectors shown in a d-q plane 60 degrees apart from each other, while $\vec{v}_0$, $\vec{v}_7$ are the two zero vectors not shown in the figure. The numbers 1-6 around the center are the sector numbers.

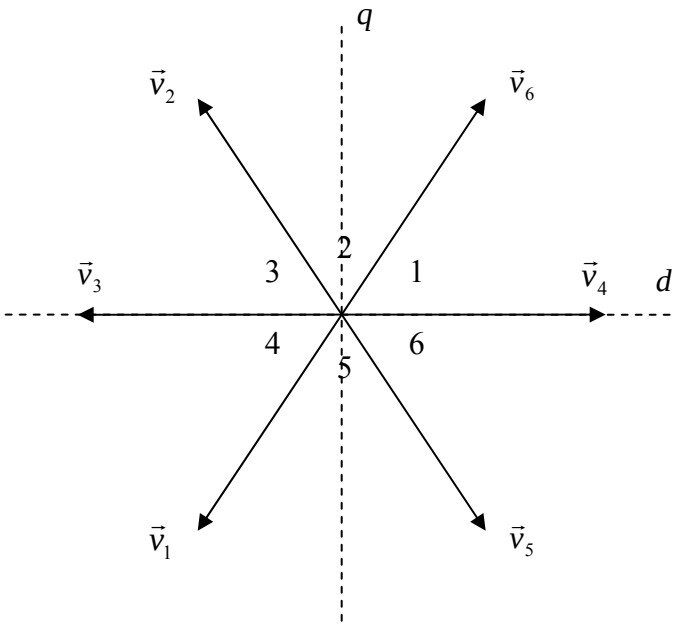

Figure 2.2 The real voltage space vectors of a voltage source inverter in the d-q plane.

For a voltage source inverter shown in Figure 2.3, the phase voltages can be expressed as following [10]

$$\begin{bmatrix} v_a \\ v_b \\ v_c \end{bmatrix} = \frac{V_{dc}}{3} \begin{bmatrix} 2 & -1 & -1 \\ -1 & 2 & -1 \\ -1 & -1 & 2 \end{bmatrix} \begin{bmatrix} a \\ b \\ c \end{bmatrix} \tag{2.6}$$

where v_a, v_b and v_c are the output phase voltages, V_{dc} is the input DC link voltage. a, b and c are the switching signals corresponding to the 3 phases with a value of "0" or "1". The "0" means that the upper power switch of the leg is off and the lower power switch is on, while "1" means the opposite, with the upper switch on and the lower switch off.

There are six real states and two zero states for these three variables, represented in a form of binary numbers $(abc)_2$ of 0 - 7. Among the eight states, state 0 and 7 are zero states because there is no voltage output from inverter in these two states.

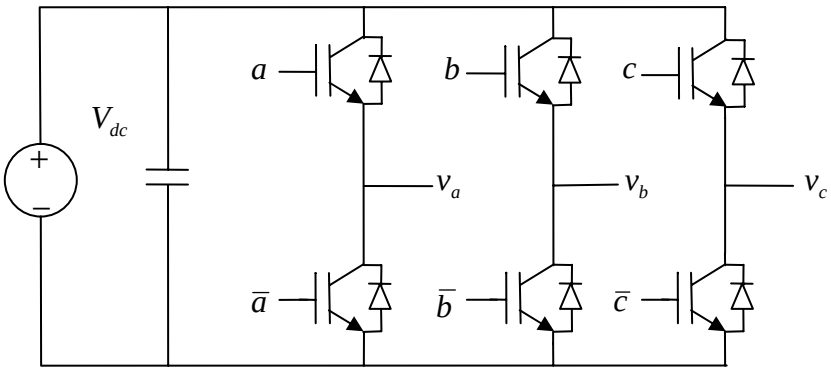

Figure 2.3 Power circuit diagram of a 3-phase voltage source inverter.

2.2 Model of Induction Motors

Neglecting the motor core loss, the saturation, the slot effect, etc, the equivalent circuit of the IM in stationary reference frame is shown in Figure 2.4. The mathematical model in this frame then can be derived from the equivalent circuit, that is,

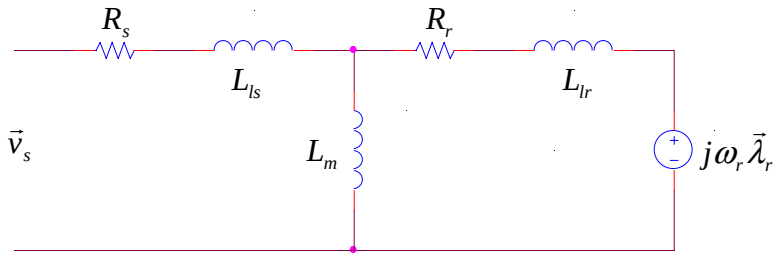

Figure 2.4 The equivalent circuit of IMs (T-model) in the stationary reference frame.

$$\vec{v}_s = R_s \vec{i}_s + \frac{d\vec{\lambda}_s}{dt} \tag{2.13}$$

$$\vec{0} = R_r \vec{i}_r + \frac{d\vec{\lambda}_r}{dt} + j\omega_r \vec{\lambda}_r \tag{2.14}$$

where,

$$L_s = L_{ls} + L_m \tag{2.15}$$

$$L_r = L_{lr} + L_m \tag{2.16}$$

and

$$\vec{\lambda}_s = L_s \vec{i}_s + L_m \vec{i}_r \tag{2.17}$$

$$\vec{\lambda}_r = L_r \vec{i}_r + L_m \vec{i}_s \tag{2.18}$$

The electromagnetic torque produced in the motor is

$$T_e = \frac{2}{3} p \,\mathrm{Im}(\vec{i}_s \vec{\lambda}_s^{\,*}) \tag{2.19}$$

Finally, the motion equation with the friction neglected is

$$J \frac{d\omega_m}{dt} = T_e - T_{ld} \tag{2.20}$$

where J is the moment of inertia including motor rotor mass moment of inertia and load mass moment of inertia, that is

$$J = J_M + J_L \tag{2.21}$$

Equation (2.19) is valid for other AC motors as well and (2.20) and (2.21) are universal.

Note, there is a more complex dynamic model of IM listed in Appendix C solely for simulating a real induction motor.

2.3 Model of Permanent Magnet Synchronous Motors

A permanent magnet synchronous motor (PMSM) is a synchronous AC motor with permanent magnets mounted in the rotor. Assuming the inductances on d and q axis are the same. The equivalent circuit of a PMSM in the stationary reference frame is illustrated in Figure 2.5.

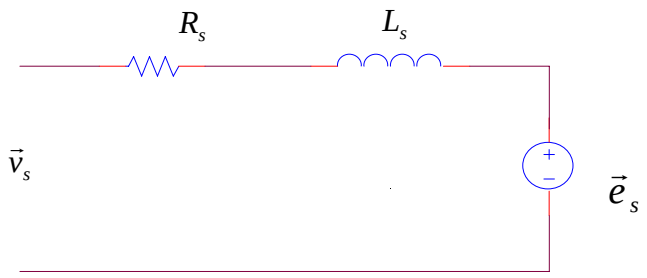

Figure 2.5 The equivalent circuit of a PMSM in the stationary reference frame.

The back EMF in the diagram is expressed as

$$\vec{e}_s = \frac{d\vec{\lambda}_f}{dt} \tag{2.20}$$

Because it is sinusoidal due to the rotor structure of this motor type,

$$\vec{\lambda}_f = \lambda_f \exp(j\theta_r) \tag{2.21}$$

Thus, the back EMF can also be written as

$$\vec{e}_s = j\omega_r \vec{\lambda}_f \tag{2.22}$$

Therefore, according to Figure 2.5,

$$\vec{v}_s = R_s \vec{i}_s + L_s \frac{d\vec{i}_s}{dt} + j\omega_r \vec{\lambda}_f \tag{2.23}$$

where

$$\vec{\lambda}_s = L_s \vec{i}_s + \vec{\lambda}_f \tag{2.24}$$

$\vec{\lambda}_f$ is the flux linkage due to the presence of the permanent magnets, its magnitude λ_f is a constant.

As mentioned in section 2.2, the torque equation (2.19) is also valid for PMSMs. And the motion equation (2.20) and inertia equation (2.21) are also the same for PMSMs. They are repeated below to complete the mathematic model.

The electromagnetic torque produced in the motor is

$$T_e = \frac{2}{3} p \,\mathrm{Im}(\vec{i}_s \vec{\lambda}_s^{\,*}) \tag{2.25}$$

The motion equation with the friction neglected is

$$J \frac{d\omega_m}{dt} = T_e - T_{ld} \tag{2.26}$$

where J is the moment of inertia including motor rotor mass moment of inertia and load mass moment of inertia, that is

$$J = J_M + J_L \tag{2.27}$$

CHAPTER III

POWER FLOW IN INDUCTION AND PERMANENT MAGNET SYNCHRONOUS MOTORS

3.1 Power Flow in Induction Motors

In the motoring mode, the IM receives electrical power from the inverter and converts it into mechanical power, but not all the input power performs the mechanical work. The input real power of IMs can be divided into two parts. One part is the electromagnetic power which is also the input power at the rotor side; the other part is the motor loss, that is,

$$P_{in} = P_e + P_{loss} \tag{3.1}$$

where P_{in} is the real input power, P_e is the electromagnetic power, P_{loss} is the stator loss. According to [11], these two powers can be further broken down, that is,

$$P_{loss} = P_{loss\_s} + P_{loss\_core} \tag{3.2}$$

$$P_e = P_{loss\_r} + P_{loss\_m} + P_{loss\_other} + P_m \tag{3.3}$$

where P_{loss_s} is the stator winding loss, P_{loss_core} is the core loss, P_{loss_r} is the rotor winding loss, P_{loss_m} is the mechanical loss, and P_m is the mechanical output power. The real power flow is illustrated in Figure 3.1.

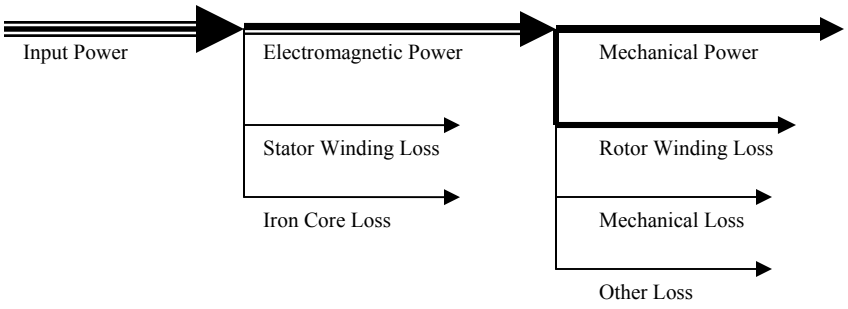

Figure 3.1 Real power flow in IMs.

The mechanical output power can be expressed as product of the generated electromagnetic torque and the mechanical angular speed:

$$P_m = T_e \omega_m = T_e \frac{\omega_r}{p} \tag{3.4}$$

Note that the electrical speed is mechanical speed multiplied by the number of pole pairs

$$\omega_r = p\omega_m \tag{3.5}$$

Similarly on the stator side [11],

$$P_e = T_e \frac{\omega_s}{p} \tag{3.6}$$

If the stator winding loss and core loss are small enough to be neglected, the input electrical power is the same as the electromagnetic power. If also the rotational losses are small and negligible, the input power can be approximated as a sum of the mechanical output power and the rotor loss of the IM. Thus,

$$P_{in} \cong P_e \cong P_m + P_{loss\_r} = P_{out} + P_{loss\_r} \tag{3.7}$$

$$P_{in} = P_e = T_e \frac{\omega_s}{p} \tag{3.8}$$

$$P_{out} = T_e \omega_m = T_e \frac{\omega_r}{p} \tag{3.9}$$

Note, the rotor loss cannot be neglected, but it can be derived from the previous formulas

$$P_{loss\_r} = P_{in} - P_{out} = \frac{T_e \omega_s}{p} - \frac{T_e \omega_r}{p} = \frac{T_e}{p}(\omega_s - \omega_r)$$

$$= s\frac{T_e \omega_s}{p} = sP_{in} \tag{3.10}$$

$$P_{out} = P_{in} - sP_{in} = (1-s)P_{in} \tag{3.11}$$

where s denotes the slip of the motor, defined as

$$s = \frac{\omega_s - \omega_r}{\omega_s} = \frac{\omega_{sl}}{\omega_s} \tag{3.12a}$$

$$s = \frac{P_{in} - P_{out}}{P_{in}} \tag{3.12b}$$

The simplified power flow after neglecting some of the losses is illustrated in Figure 3.2.

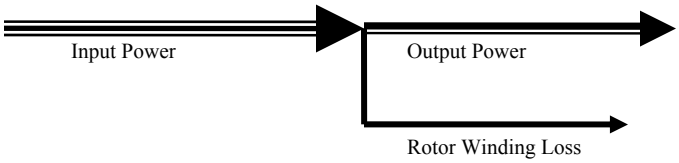

Figure 3.2 Simplified real power flow in IMs

As to reactive power, it does not do any actual work and produces no loss. Therefore there is only one input reactive power that is required for IM to operate.

Input instantaneous real power

$$P_{in} = v_a i_a + v_b i_b + v_c i_c \tag{3.13}$$

$$P_{in} = \frac{2}{3}\mathrm{Re}(\vec{v}_s \vec{i}_s^{\,*}) = \frac{2}{3}(v_{ds} i_{ds} + v_{qs} i_{qs}) \tag{3.14}$$

Input instantaneous reactive power

$$Q_{in} = \frac{2}{3}\mathrm{Im}(\vec{v}_s \vec{i}_s^{\,*}) = \frac{2}{3}(v_{qs} i_{ds} - v_{ds} i_{qs}) \tag{3.15}$$

3.2 Power Flow in PMSMs

PMSMs differ from IMs by the absence of slip. Therefore, if all losses are ignored, the input power equals the output power. According to (3.11)

$$P_{in} = P_{out} = \omega_m T_e \tag{3.16}$$

CHAPTER IV

PRINCIPLES OF DIRECT TORQUE CONTROL OF INDUCTION MOTORS

The direct power control methods discussed in this thesis bear certain similarity to the direct torque control (DTC). Therefore, principles of DTC are reviewed in this chapter before introduction of the proposed direct power control approaches.

DTC is actually direct torque and flux control, with two parameters involved in the control strategy, so it is also named as direct torque and flux control (DTFC) in some publications. DTC is a control method that directly selects inverter states based on the torque and flux errors. Hysteresis (relay) controllers are employed, and no current controllers are present. The voltage source inverter shown in Figure 4.1 in the general block diagram of direct torque and flux control system will be used in all systems considered in this thesis. Figure 4.2 depicts a detailed DTC system diagram.

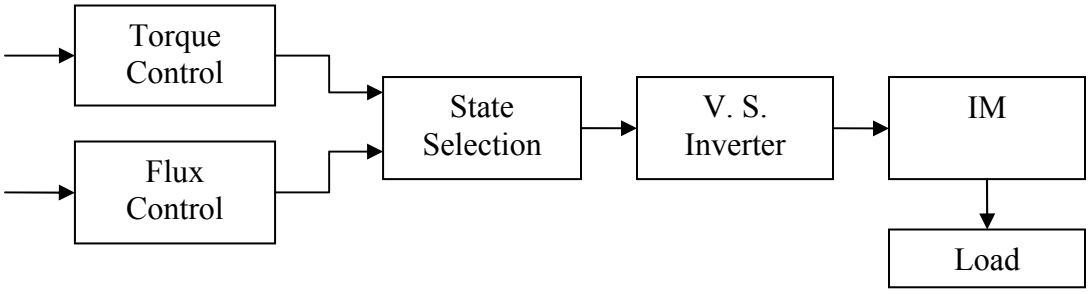

Figure 4.1 Block diagram of direct torque and flux control system.

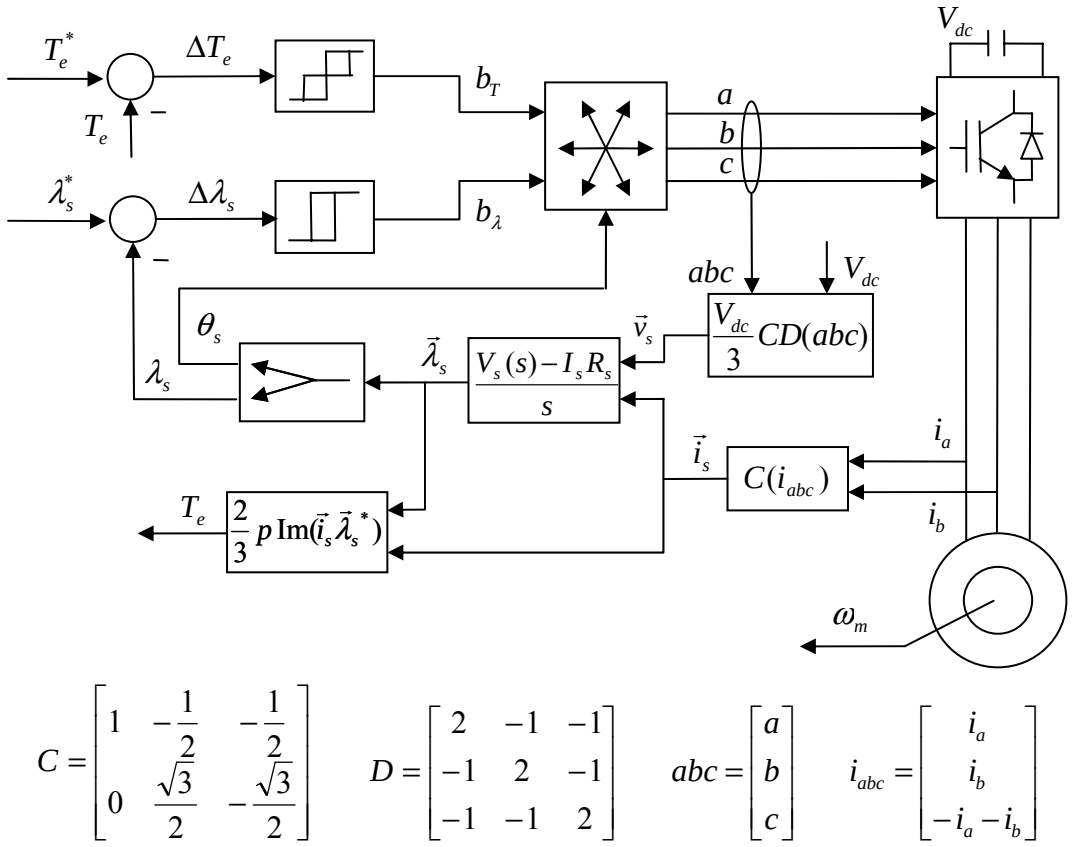

Figure 4.2 Direct torque and flux control system without a speed control loop.

4.1 Flux Control Principles

Flux linkage is very important in IMs. Constant flux can provide enough electromagnetic torque and avoid magnetizing current saturation in the iron core of the IM. Therefore in direct torque and flux control, as well as in the proposed direct power and flux controls in the subsequent chapters, the flux is maintained constant.

In the stator stationary reference frame, the frame rotation speed is zero and the rotor voltage is zero as well (for squirrel-cage IMs), thus (2.1) and (2.2) can be used to describe this type of motors. They are repeated below for the convenience:

$$\vec{v}_s = R_s \vec{i}_s + \frac{d\vec{\lambda}_s}{dt} \tag{4.1}$$

$$\vec{0} = R_r \vec{i}_r + \frac{d\vec{\lambda}_r}{dt} - j\omega_r \vec{\lambda}_r \tag{4.2}$$

If we neglect the small voltage drop across the stator resistance, we have

$$\vec{v}_s \cong \frac{d\vec{\lambda}_s}{dt} \tag{4.3}$$

Integrating (4.3) and writing it in a discrete form, we obtain

$$\vec{\lambda}_s(t_{n+1}) = \vec{\lambda}_s(t_n) + \vec{v}_s \Delta t \tag{4.4}$$

that is,

$$\Delta\vec{\lambda}_s \cong \vec{v}_s \Delta t \tag{4.5}$$

where $\Delta t = t_{n+1} - t_n$ equals the switching interval.

Therefore, within a switching interval Δt , the increase of stator flux is proportional to the stator voltage space vector. This is the principle of direct flux control in DTC.

4.2 Electromagnetic Torque Control Principles

The electromagnetic torque generated in motors is a key parameter responsible for the dynamic performance of electric drive systems. In traditional motor control methods

such as FOC, it is indirectly controlled through the control of current. In DTC, it is controlled directly by selection of the inverter states.

The stator and rotor current vectors are given by

$$\vec{i}_s = \frac{\vec{\lambda}_s - L_m \vec{i}_r}{L_s} \tag{4.6}$$

$$\vec{i}_r = \frac{\vec{\lambda}_r - L_m \vec{i}_s}{L_r} \tag{4.7}$$

Substituting (4.7) in (4.6) yields

$$\vec{i}_s = \frac{L_r \vec{\lambda}_s - L_m \vec{\lambda}_r}{L_s L_r - L_m{}^2} \tag{4.8}$$

By substituting (4.8) in (2.19), the electromagnetic torque generated in the IM can be expressed as

$$T_e = \frac{2}{3} p \,\mathrm{Im}(\vec{i}_s \vec{\lambda}_s{}^*) = \frac{2}{3} p \,\mathrm{Im}\left(\frac{L_r \vec{\lambda}_s - L_m \vec{\lambda}_r}{L_s L_r - L_m{}^2} \vec{\lambda}_s{}^* \right)$$

$$= -\frac{2}{3} p \frac{L_m}{L_\sigma{}^2} \mathrm{Im}(\vec{\lambda}_r \vec{\lambda}_s{}^*) = \frac{2}{3} p \frac{L_m}{L_\sigma{}^2} \mathrm{Im}(\vec{\lambda}_s \vec{\lambda}_r{}^*)$$

$$= \frac{2}{3} p \frac{L_m}{L_\sigma{}^2} \lambda_s \lambda_r \sin(\theta_s - \theta_r) \tag{4.9}$$

where $L_\sigma{}^2 = L_s L_r - L_m{}^2$.

Rotor flux is inertial comparing with the stator flux, so within a small sampling interval Δt, it can be considered constant. Then torque can be controlled by changing the stator flux angle θ_s which is affected by the voltage vectors shown in Figure 4.3.

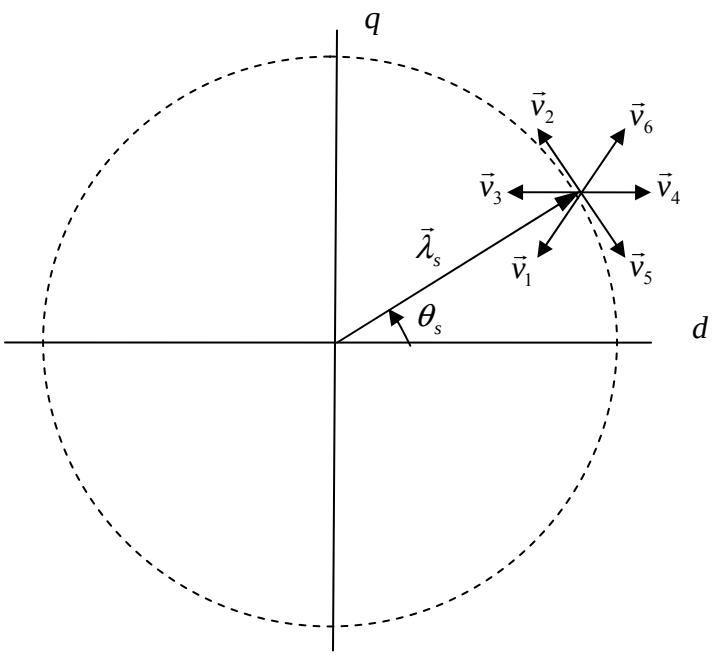

Figure 4.3 Illustration of torque and flux control through selection of voltage vectors in a stationary d-q frame.

4.3 Implementation of the DTC

As depicted in Figure 4.2, two binary outputs from the torque and stator flux controller are taken as inputs for a switching variable selection table, the output of which is also dependent on the angular position of the stator flux. Then this three-digit switching variable output is employed to switch the 3-phase inverter MOSFETs or IGBTs. Detailed discussion of the implementation of the direct control method will be found in the subsequent chapters.

CHAPTER V

DIRECT POWER AND FLUX CONTROL OF INDUCTION MOTORS

Direct power and flux control (DPFC) of IMs is a control method that directly selects output voltage vector states based on the power and flux errors using hysteresis controllers. In this respect, the method is similar to DTC described in Chapter IV.

Figure 4.1 shows the block diagram of a general open-loop DPFC system, while Figure 4.2 illustrates a more detailed block diagram of the same open-loop DPFC control system. It consists of a three-level hysteresis power controller, a two-level hysteresis flux controller, a state selection look-up table, an actual power estimator, an actual flux estimator, a voltage and current vector assembler, a voltage source inverter, and an IM.

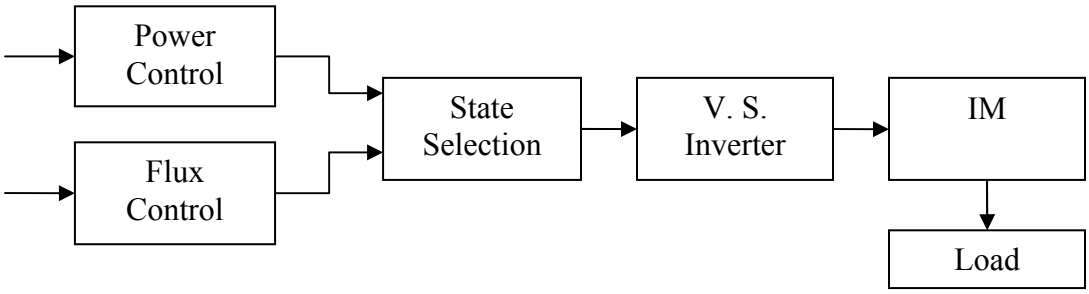

Figure 5.1 A general block diagram of direct power and flux control system.

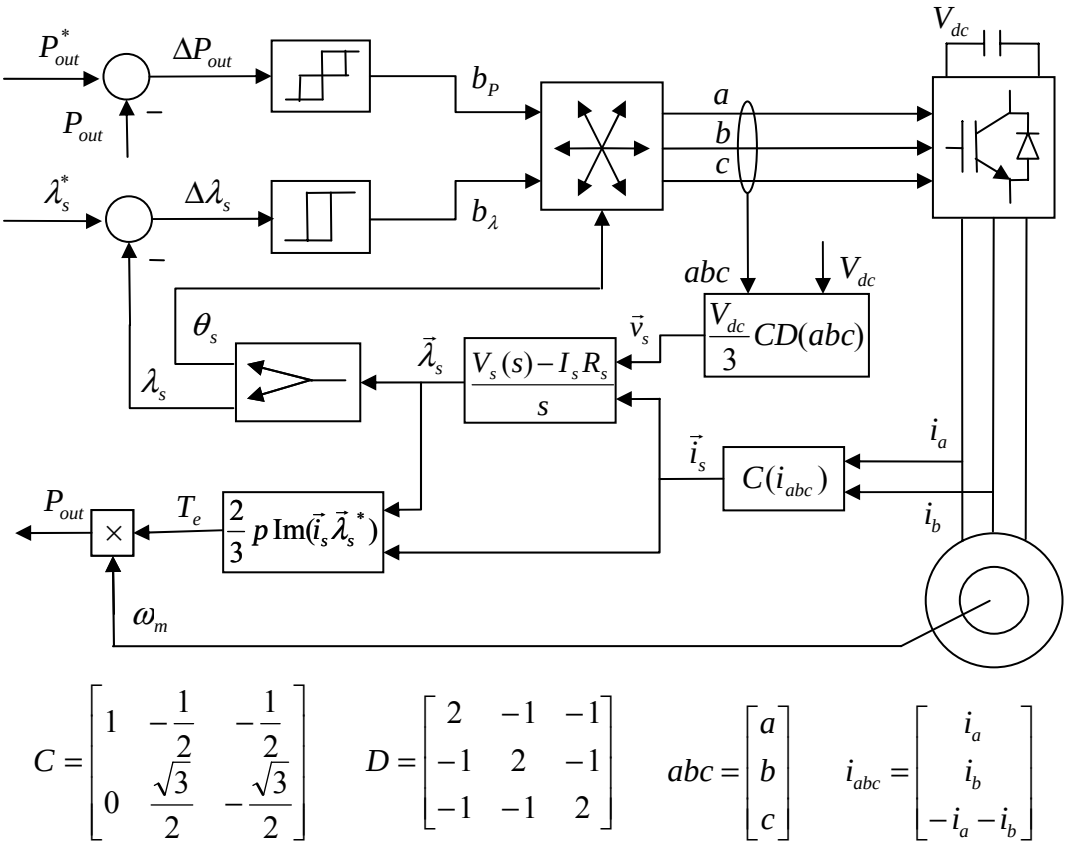

Figure 5.2 The direct output power and flux control system without a speed loop.

5.1 Flux Control Principles

In DPFC, the flux is still maintained constant and the control principles of the flux are the same as that in DTC (refer to Section 4.1for details).

5.2 Power Control Principles

From the power flow charts in Chapter III, it is evident that real output power is the part that produces the torque, and is what the user of the system is mostly interested in. The output real power is given by

$$P_{out} = T_e \frac{\omega_r}{p} \tag{5.1}$$

Substituting the torque in (5.1) with (4.9), the output power becomes

$$P_{out} = \frac{2}{3}\omega_r \frac{L_m}{L_\sigma{}^2} \mathrm{Im}(\vec{\lambda}_s \vec{\lambda}_r{}^*)$$

$$= \frac{2}{3}\frac{L_m}{L_\sigma{}^2}\omega_r \lambda_s \lambda_r \sin(\theta_s - \theta_r) \tag{5.2}$$

Since the magnitude of the stator flux is kept constant and the rotor flux does not change much due to its inertia, the rotor speed and angle can be considered constant too. The formula above shows that the change of output power depends only on the change of stator flux angle. The stator voltage vector that can increase the stator angle needs to be raised in order to increase the output power.

The real output power equation obtained above is only valid for explanation of the principles of power control. However, it is not appropriate for the purpose of estimating the actual power in simulations.

5.3 Output Power Reference

The output power reference is the command value, or set point, for the power control. In a closed-loop speed control system, the reference of the power controller is obtained from the output of the PI-type speed controller (see Figure 5.3).

The speed error is defined as the difference of the reference speed and the estimated actual speed

$$\Delta\omega_m = \omega_m^* - \omega_m \tag{5.3}$$

where ω_m^* is the reference speed (the asterisk denotes a reference value). Then, the reference torque can be obtained through a conventional PI controller as

$$T_e^* = K_p(\Delta\omega_m) + K_i\int(\Delta\omega_m)dt \tag{5.4}$$

The continuous standard form above can also be expressed in a discrete incremental PI control form, which is more suitable for the digital implementation.

$$T_e^*(t_{n+1}) = T_e^*(t_n) + K_p[\Delta\omega_m(t_n) - \Delta\omega_m(t_{n-1})] + K_i\Delta T\Delta\omega_m(t_n) \tag{5.5}$$

The subscript *(n)* denotes the current sampling instant, *(n-1)* is the last instant, and *(n+1)* is the next one. The proportional gain is denoted by K_p, K_i is the integral gain, which equals K_p divided by the integral time constant T_i, and ΔT is the sampling time interval between the *n* and *(n+1)* sampling instants. The output power reference according to (3.9) is therefore expressed as

$$P_{out}^* = T_e^*\omega_m^* \tag{5.6}$$

The process of obtaining the output power reference from the speed reference is illustrated in Figure 5.3.

For simulations, the actual motor speed ω_m can be obtained as

$$\omega_m = \frac{1}{J}\int(T_e - T_{ld})dt \tag{5.7}$$

In practice the speed is either measured directly or estimated from the current and voltage signals. The magnitude of the stator flux is kept constant in the simulation, thus the flux reference λ_s^* is a constant. The error of the stator flux is

$$\Delta\lambda_s = \lambda_s^* - \lambda_s \tag{5.8}$$

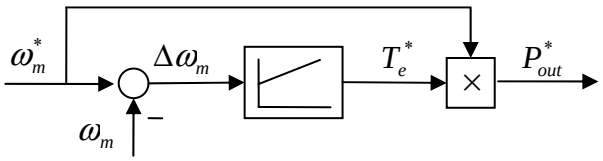

Figure 5.3 Diagram of output power reference obtained from speed loop.

5.4 Power and Flux Hysteresis Controllers

Both the output power and the stator flux controllers are of hysteresis type. Depending on the control error, the output of the controller is set to two or three discrete values. The power controller has a three level output. The values are 1, 0 and -1, representing an increase, no change, and a decrease of the controlled variable, respectively. The number of flux controller output levels is two, with 1 and 0 meaning an increase and decrease commands, respectively. Figure 5.4 illustrates characteristics of these two controllers.

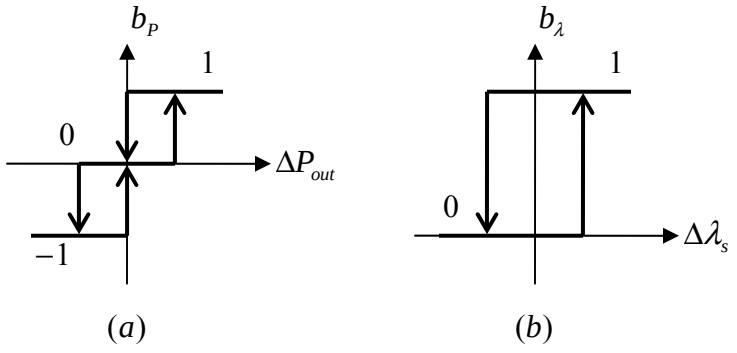

Figure 5.4 Characteristics of the hysteresis controllers: (a) power controller, (b) flux controller.

The mathematical description of the controllers is given below. The power controller's output is given by

$$b_P = \begin{cases} 1 & (\Delta P_{out} \geq P_{th}); or (\Delta P_{out} > 0) and (\dfrac{d\Delta P_{out}}{dt} < 0) \\ -1 & (\Delta P_{out} \leq -P_{th}); or (\Delta P_{out} < 0) and (\dfrac{d\Delta P_{out}}{dt} > 0) \\ 0 & Otherwise \end{cases} \tag{5.9}$$

and that of the flux controller, by

$$b_\lambda = \begin{cases} 1 & (\Delta \lambda_s \geq \lambda_{th}); or (-\lambda_{th} < \Delta \lambda_s < \lambda_{th}) and (\dfrac{d\Delta P_{out}}{dt} < 0) \\ 0 & Otherwise \end{cases} \tag{5.10}$$

The thresholds of the power and stator flux are denoted by P_{th} and λ_{th} respectively. The smaller the thresholds, the finer the control is, but the switching rate goes up.

5.5 State Selection

The task of the state selector in the direct power control is to combine the outputs of the power controller and flux controller to select the values of the switching variables *a*, *b*, and *c*. These variables describe the required voltage vectors of the inverter.

To make it easier to implement, the combination of the two controller outputs can be expressed as follows:

$$b = 3b_\lambda + b_P + 2 \tag{5.11}$$

In the above equation, the variable b = 1, 2, 3, 4, 5, 6, while b_λ = (0, 1) and b_P = (-1, 0, 1). Alternatively, (5.11) can also be represented by Table 5.1.

Table 5.1 Combination of the power and flux controller outputs

b	$b_P = -1$	$b_P = 0$	$b_P = 1$
$b_\lambda = 0$	1	2	3
$b_\lambda = 1$	4	5	6

A whole stator flux cycle of 360º is divided equally into 6 sectors, each one spanning 60º. Combining with the sector numbers from 1 through 6, produces the look-up Table 5.2 for the state selection. The concept of state selection is illustrated in Figure 5.5.

Table 5.2 State selection loop-up table

	$b = 1$	$b = 2$	$b = 3$	$b = 4$	$b = 5$	$b = 6$
Sector 1	1	0	2	5	7	6
Sector 2	5	7	6	4	0	2
Sector 3	4	0	1	6	7	3
Sector 4	6	7	5	2	0	1
Sector 5	2	0	4	3	7	5
Sector 6	3	7	6	1	0	4

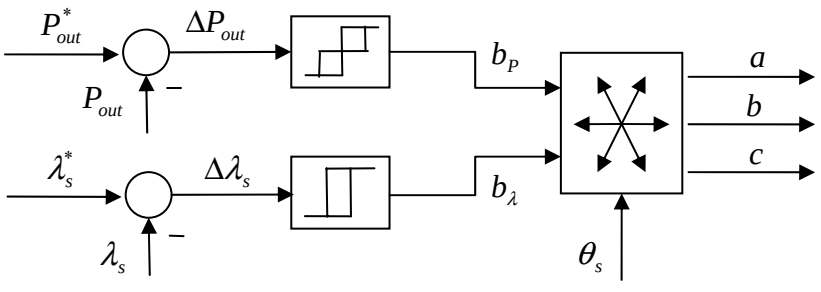

Figure 5.5 Block diagram of the inverter state selection.

Note that the stator flux angle θ_s must be converted to a sector number of 1 through 6 for the use of Table 5.2 for state selection.

5.6 Estimation of Stator Flux and Output Power

The estimation of flux is implemented by integration of (4.1):

$$\vec{\lambda}_s = \int (\vec{v}_s - \vec{i}_s R_s) dt \tag{5.12}$$

and the speed estimation is based on (2.11), so that the estimated output power can be obtained from (3.9). Figure 4.6 illustrated the estimation of the actual output power and flux from stator voltage and current together with mechanical angular speed. These estimated values are the feedbacks for the output power and stator flux controls shown in Figure 5.6.

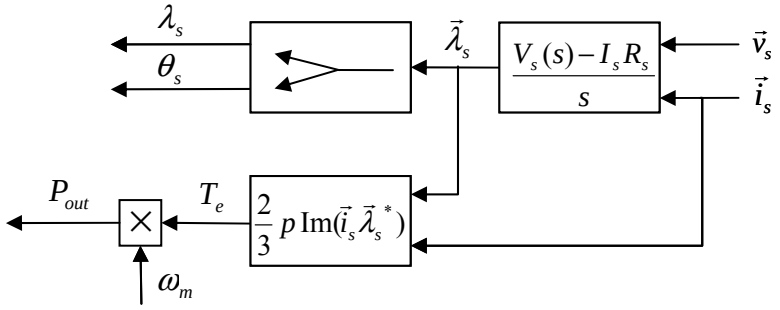

Figure 5.6 Estimation of actual output power and stator flux linkage

5.7 Simulation Results

The simulation was carried out using MATLAB. The whole system setup is shown in Figure 5.7. It can be seen that this is a power and flux dual-controller system. While the flux control has only one loop, a speed loop is present outside the power control.

The sampling frequency was chosen as 50 kHz and the switching frequency was no higher than the sampling frequency. The hesteresis tolerance for both control of outpur power and stator flux linkage was 1% of their respective reference values. The relative tolerance was used because it can improve the control quality, increase the system stability at low motor speeds and reduce the unnecessary switchings at higher speeds as well. The absolute thresholds of 1 W power and 0.01 Wb were also tested with similar result. .For the PI speed controller (see Equation 5.4), the propertional gain was tuned to $K_p = 90$, the overall coefficient of the integral part was set to 0.1, which yielded an integral gain $K_i = 5000$ at the 50 kHz sampling rate. The reference speed profile was such that the speed was always kept below the rated speed to avoid field weakening. The parameters of the IM used in the simulations are listed in Appendix A.

First, a constant mechanical load of 90 Nm was assumed at all times, including the starting stage. The load corresponded to approximately half of the motor rated torque. Next, an almost full load of 180 Nm was applied. The simulation results are shown in Figures 5.8 through 5.13. Waveforms of interest under these two load conditions are placed next to each other for easy comparison. The magnitude of flux was kept constant at 1.2 Wb.

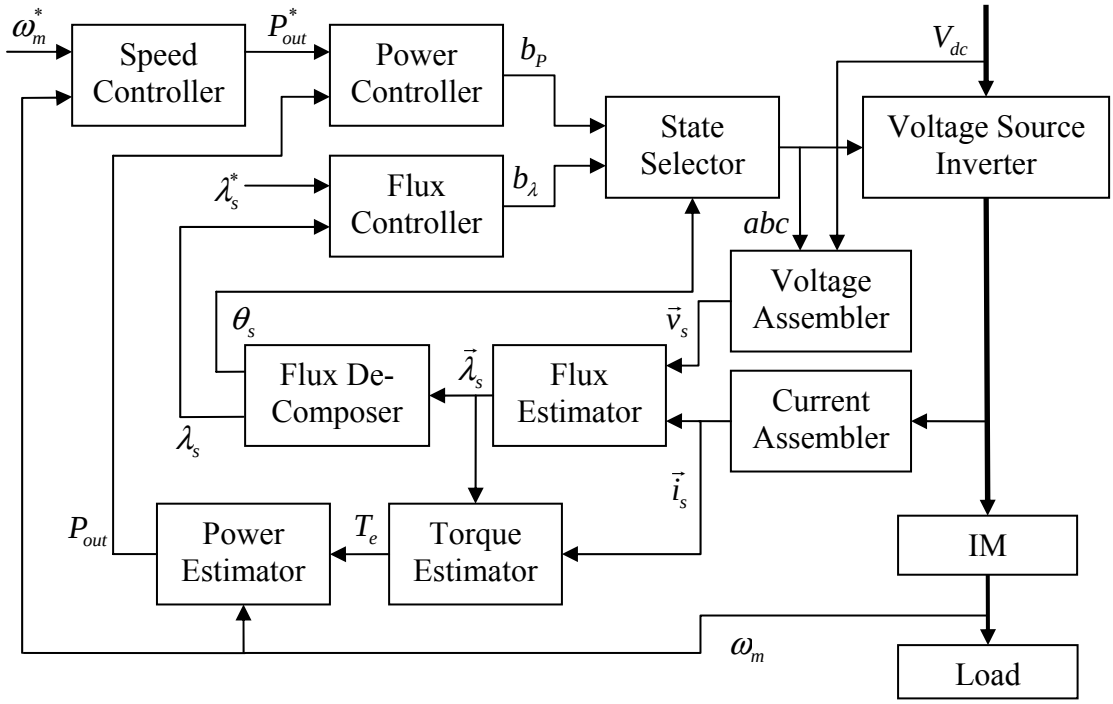

Figure 5.7 Block diagram of the direct outpower and flux control system for IM with closed-loop speed control.

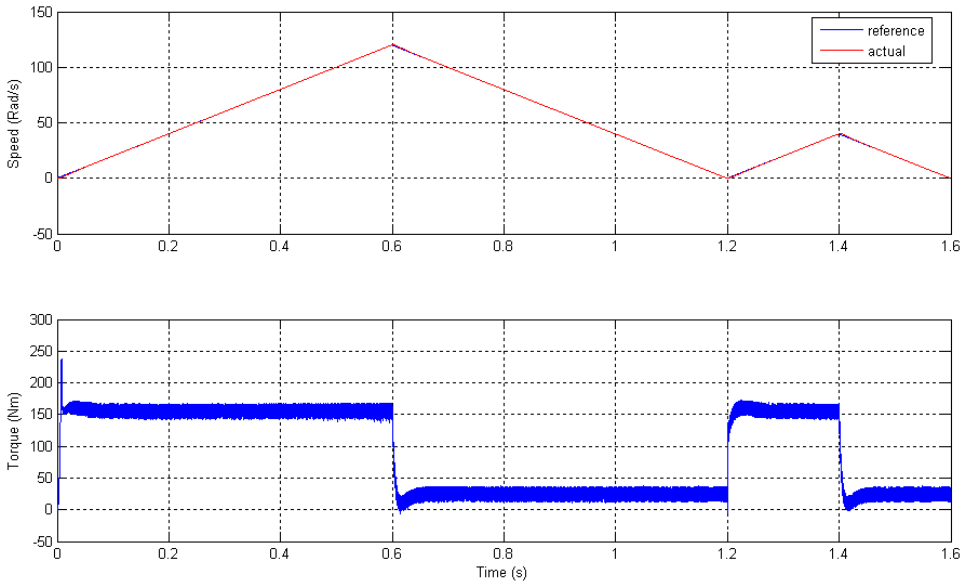

Figure 5.8 Speed and torque in IM direct output power and flux control: half load.

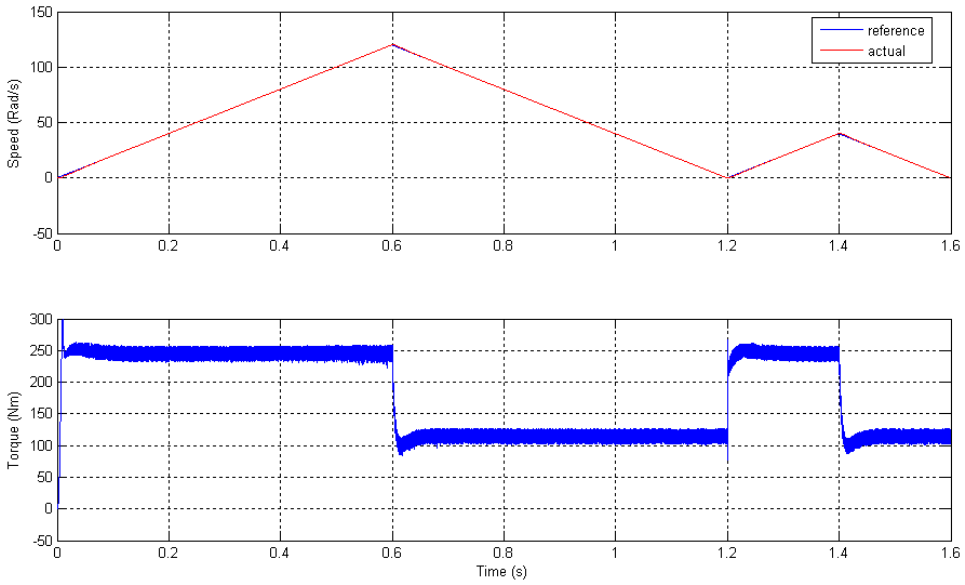

Figure 5.9 Speed and torque in IM direct output power and flux control: full load.

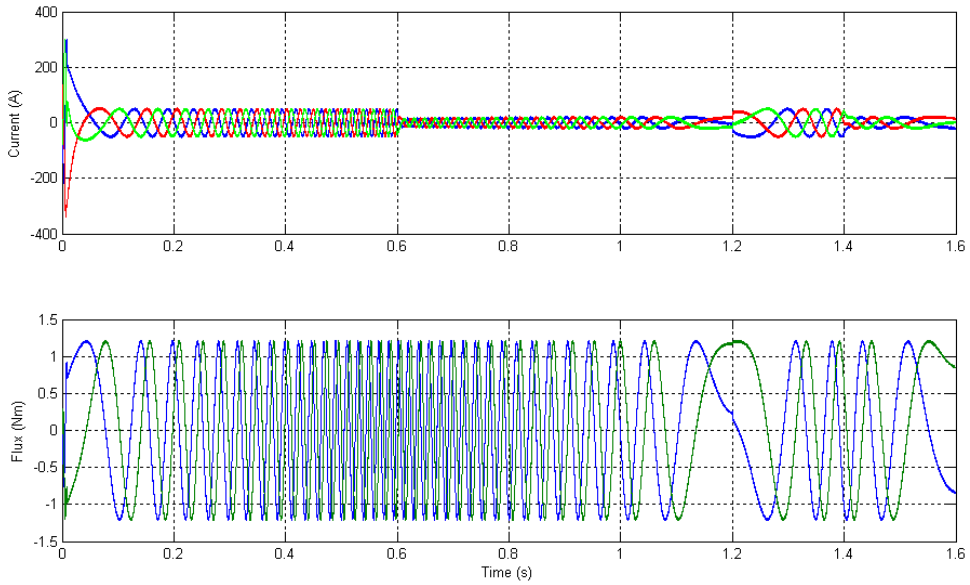

Figure 5.10 Stator currents and flux in IM direct power and flux control: half load.

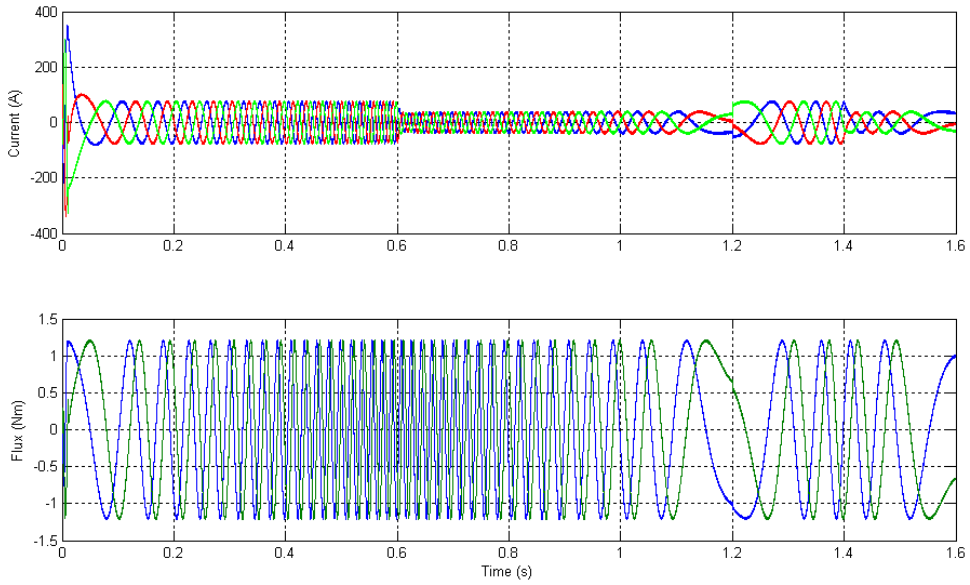

Figure 5.11 Stator currents and flux in IM direct power and flux control: full load.

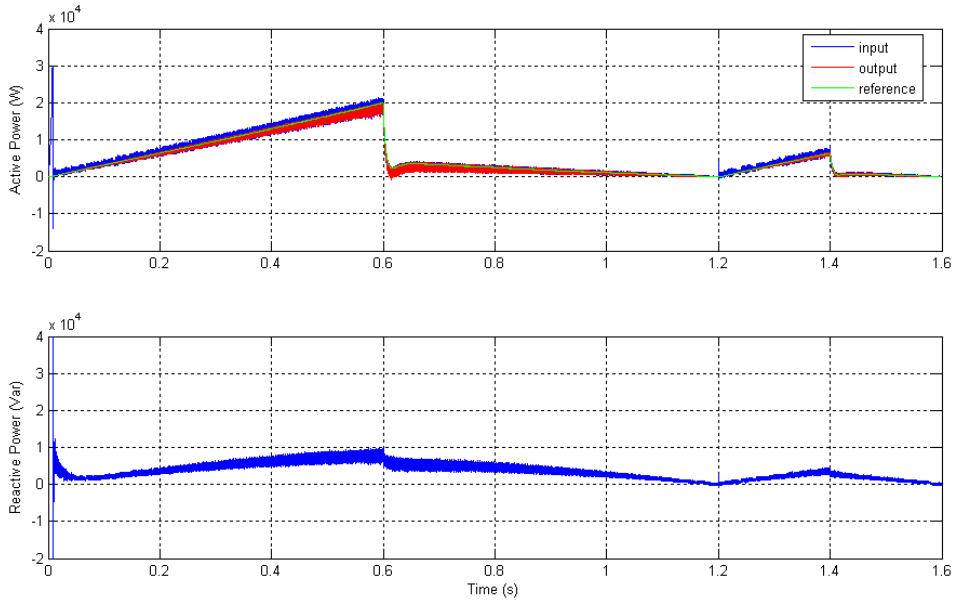

Figure 5.12 Real and reactive power in IM direct power and flux control: half load.

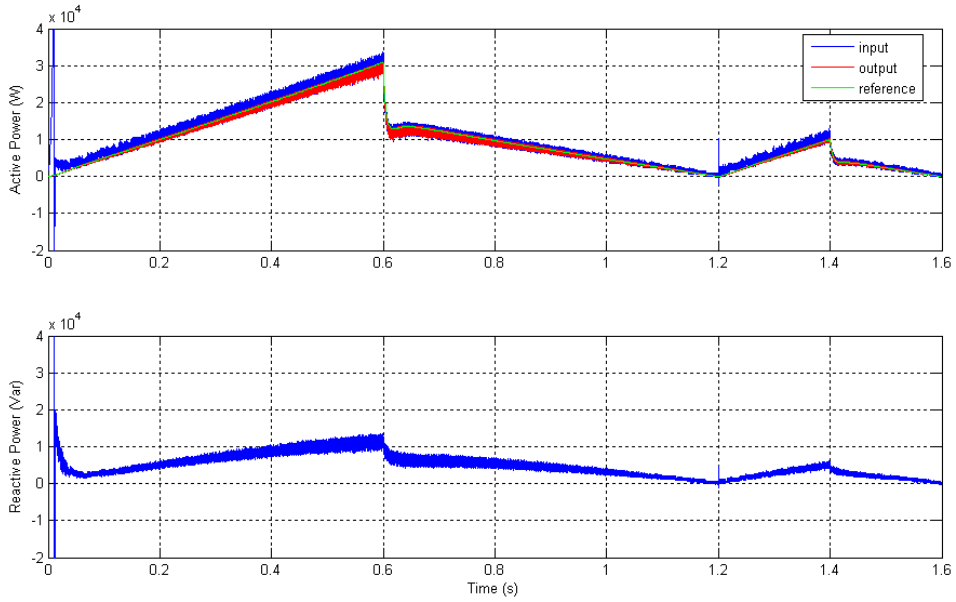

Figure 5.13 Real and reactive power in IM direct power and flux control: full load.

CHAPTER VI

DIRECT INPUT POWER AND FLUX CONTROL OF INDUCTION MOTORS

The flux control in direct input power and flux control of IMs remains exactly the same as in the output power and flux control, thus only the principles of input power control will be discussed in this chapter.

6.1 Principles of Input Power Control

Substituting the electromagnetic torque in (3.7) with the right-hand side of (2.12), the input power is derived as follows:

$$P_{in} = T_e \frac{\omega_s}{p} = T_e \frac{\omega_r + \omega_{sl}}{p}$$

$$= \frac{2}{3} \frac{L_m}{L_\sigma^{\,2}} \omega_s \, \mathrm{Im}(\vec{\lambda}_s \vec{\lambda}_r^{\,*})$$

$$= \frac{2}{3} \frac{L_m}{L_\sigma^{\,2}} \omega_s \lambda_s \lambda_r \sin(\theta_s - \theta_r) \qquad (6.1a)$$

$$= \frac{2}{3} \frac{L_m}{L_\sigma^{\,2}} (\omega_r + \omega_{sl}) \lambda_s \lambda_r \sin(\theta_s - \theta_r) \qquad (6.1b)$$

$$= \frac{2}{3} \frac{L_m \omega_r}{L_\sigma^{\,2}} \lambda_s \lambda_r \sin(\theta_s - \theta_r) + \frac{2}{3} \frac{L_m \omega_{sl}}{L_\sigma^{\,2}} \lambda_s \lambda_r \sin(\theta_s - \theta_r) \qquad (6.1c)$$

The first term of the (6.1c) is the output power. The second term's size is dependent on the slip speed, which in the steady state is small. However, in transient states, the second term cannot be ignored. It depends on the extent of change of operating conditions.

6.2 Input Power Reference

Comparing (6.1b) with (5.2), we can see that they differ by the slip-speed part of the real power. When we try to control the input real power directly, the slip speed part must be compensated properly in the reference in order to get the desired control effect. Therefore, the input real power consists of two parts: the output power part and the slip-speed part.

The output power part would remain the same as in the output power control, but the slip speed part is not easy to determine [6]. To estimate it, we assume the reference slip speed to be proportional to the speed control error. This assumption is justified by the fact that for the motor to catch up with the reference speed, the error causes a torque change, which affects the slip speed. Thus we have,

$$\omega_{sl}^{*} = k_{sl}\Delta\omega_m = k_{sl}(\omega_m^{*} - \omega_m) \tag{6.2}$$

The gain parameter k_{sl} can be predetermined and adjusted during simulations. Note, this method is just a simple way to compensate for the slip speed. Then the input power reference is given as

$$P_{in}^{*} = T_e^{*}(\omega_m^{*} + \omega_{sl}^{*}) = T_e^{*}(\omega_m^{*} + k_{sl}\Delta\omega_m) \tag{6.3}$$

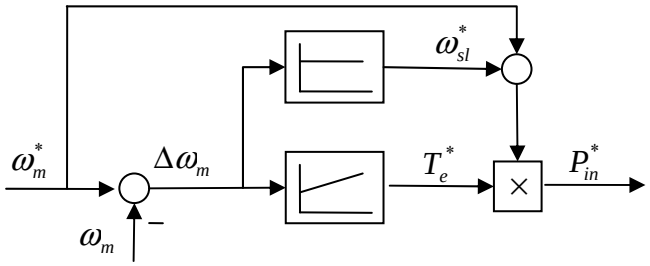

Figure 6.1 Block diagram of the input power reference obtained from the speed loop.

6.3 Input Power Estimation

For the actual input power estimation, (3.14) can be employed, as information about the stator voltage and current can be easily obtained. However, it has been found through simulations that the system can easily get unstable. That gave rise to the successful idea of using stator flux instead, as the flux is approximately the integral of the stator voltage.

If stator resistance is neglected, the stator voltage is

$$\vec{v}_s \cong \frac{d\vec{\lambda}_s}{dt} = \frac{d[\lambda_s \exp(j\theta_s)]}{dt} \tag{6.4}$$

When the magnitude of the flux is kept constant, it becomes

$$\vec{v}_s = \lambda_s \frac{d[\exp(j\theta_s)]}{dt}$$

$$= j\frac{d\theta_s}{dt}\lambda_s \exp(j\theta_s)$$

$$= j\omega_s\lambda_s \exp(j\theta_s) = j\omega_s\vec{\lambda}_s \tag{6.5}$$

Substituting (6.5) in (3.14), the actual input power estimation yields

$$P_{in} = \frac{2}{3}\mathrm{Re}(\vec{v}_s \vec{i}_s^{\,*})$$

$$= \frac{2}{3}\mathrm{Re}(j\omega_s \vec{\lambda}_s \vec{i}_s^{\,*})$$

$$= \frac{2\omega_s}{3}\mathrm{Re}\left[j(\lambda_{ds} + j\lambda_{qs})(i_{ds} - ji_{qs})\right]$$

$$= \frac{2\omega_s}{3}(\lambda_{ds} i_{qs} - \lambda_{qs} i_{ds}) \qquad (6.6)$$

The stator flux estimation can be obtained from (4.1) by integration. The stator electrical speed ω_s is estimated from (6.7) [11] as

$$\omega_s = \frac{\frac{d\lambda_{qs}}{dt}\lambda_{ds} - \frac{d\lambda_{ds}}{dt}\lambda_{qs}}{(\lambda_{ds}^{\,2} + \lambda_{qs}^{\,2})} = \frac{\frac{d\lambda_{qs}}{dt}\lambda_{ds} - \frac{d\lambda_{ds}}{dt}\lambda_{qs}}{\lambda_s^{\,2}} \qquad (6.7)$$

Note, that the estimation of stator speed from (6.7) is very noisy due to the derivative terms. A filter has to be applied to the stator speed before it can be used in the estimation of the real power in (6.6). In the simulations, a simple sliding-window averaging filter has been used. Notice the difference of input power estimation in Figure 6.2 from the input power estimation in Figure 5.3.

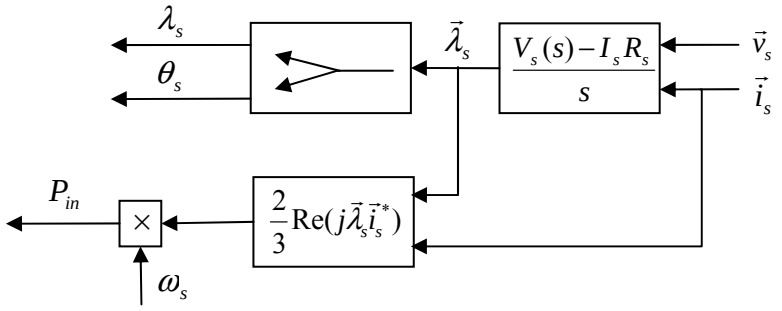

Figure 6.2 Estimation of actual input real power and stator flux linkage

6.4 Simulation Results

The simulation setup of the input real power and flux control, shown in Figure 6.3, has a similar structure as that of the output real power and flux control, which has been illustrated in Figure 5.7. The two differences are: (1) all powers are input power and (2) the speed used for actual power estimation is the stator angular speed. Consequently, contents of some function blocks are different too. The simulation assumed the same conditions as in the case of the IM output power and flux control, that is, the same speed profile, the same load, the same parameters of the PI speed controller, and the same sampling frequency. The gain for slip speed reference was chosen as $K_{sl} = 3$ (see (6.2)).

It is needed to mention that this input power control does not work with absolute thresholds, whereas the other successful approaches in this thesis do.

Similarly to the output power control, the simulation results for the IM direct input power and flux control with a half load of 90 Nm and a full load of 180 Nm conditions are shown in Figures 6.4 through 6.9.

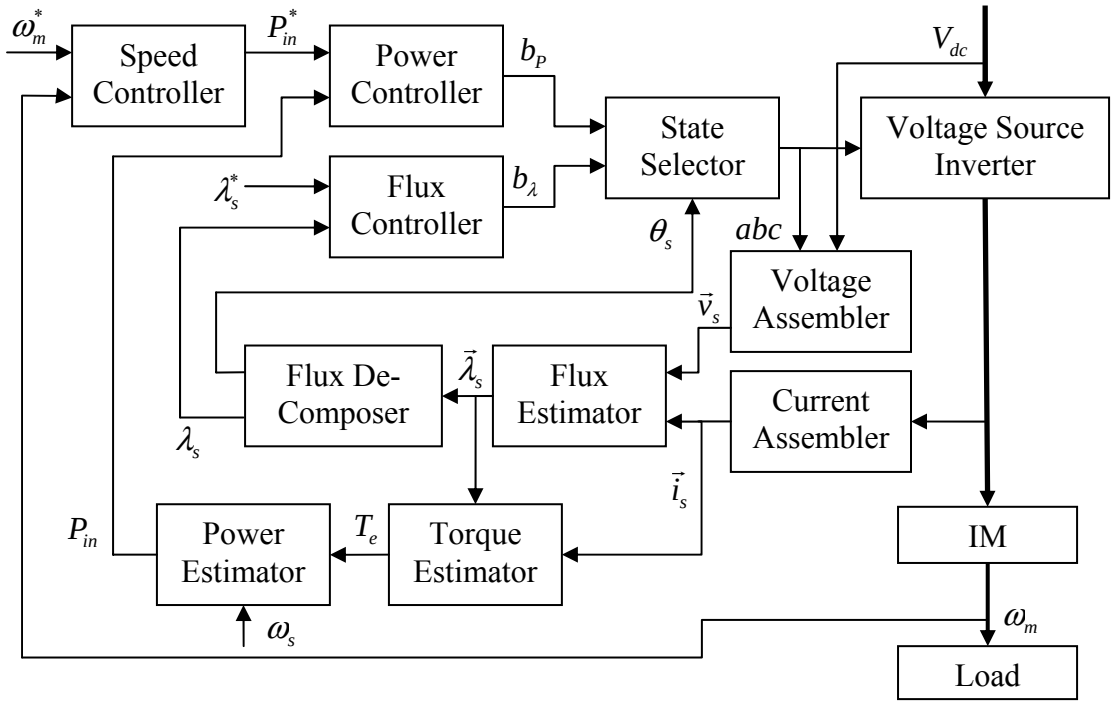

Figure 6.3 Block diagram of the direct input power and flux control system for IM with closed-loop speed control.

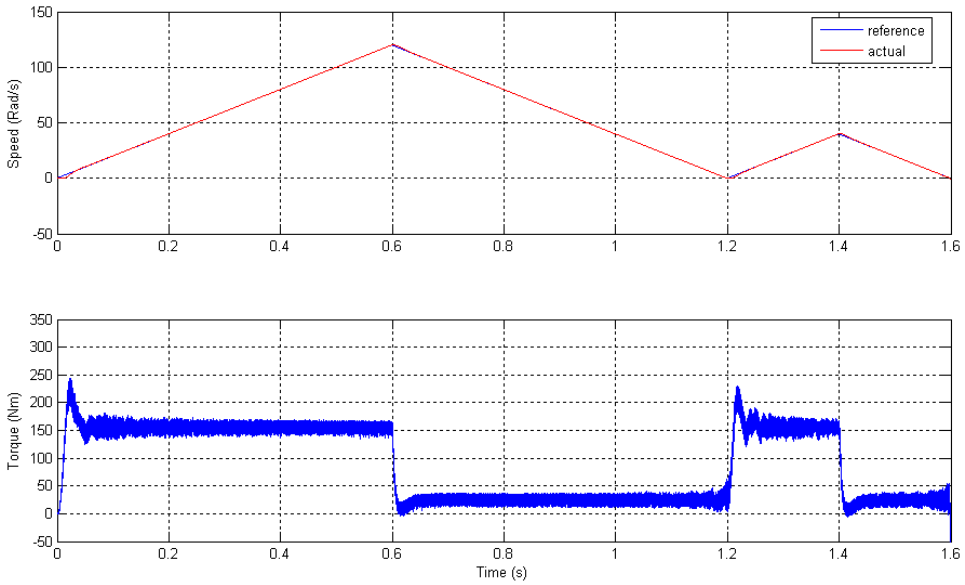

Figure 6.4 Speed and torque in IM direct input power and flux control: half load.

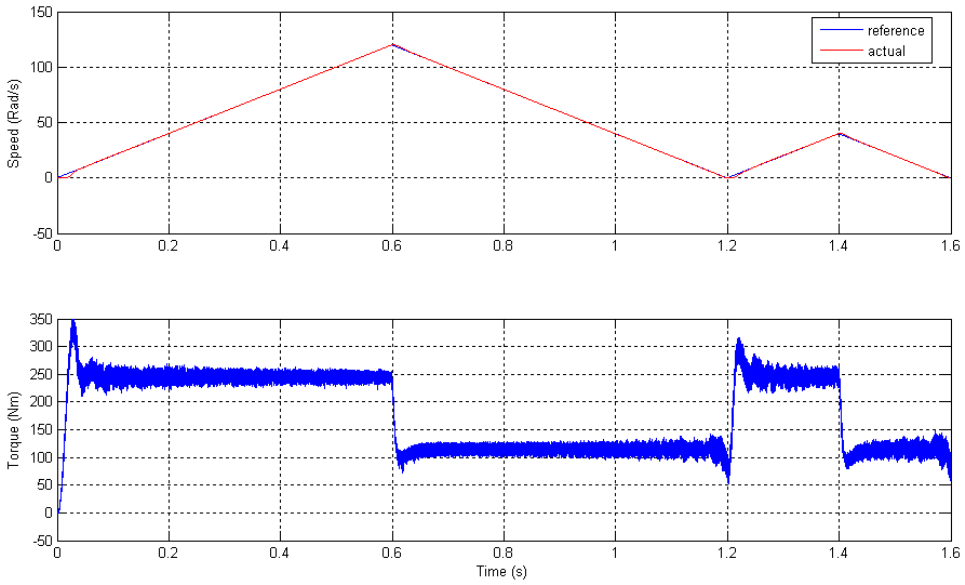

Figure 6.5 Speed and torque in IM direct input power and flux control: full load.

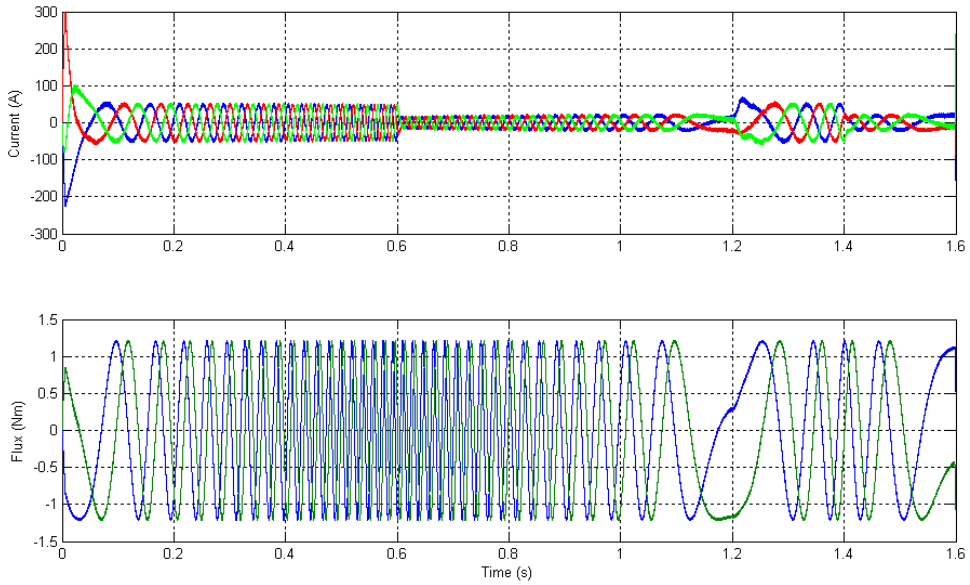

Figure 6.6 Stator currents and flux in IM direct input power and flux control: half load.

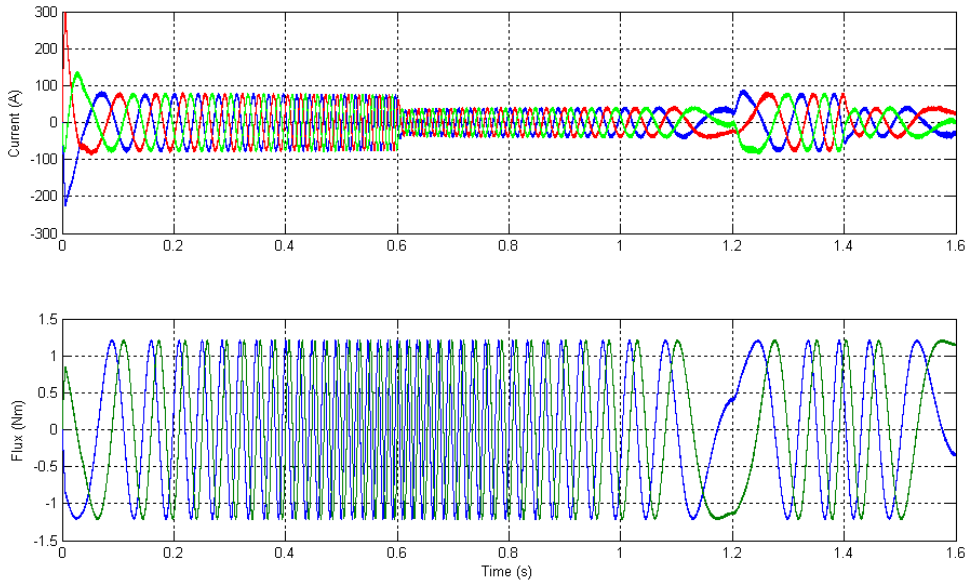

Figure 6.7 Stator currents and flux in IM direct input power and flux control: full load.

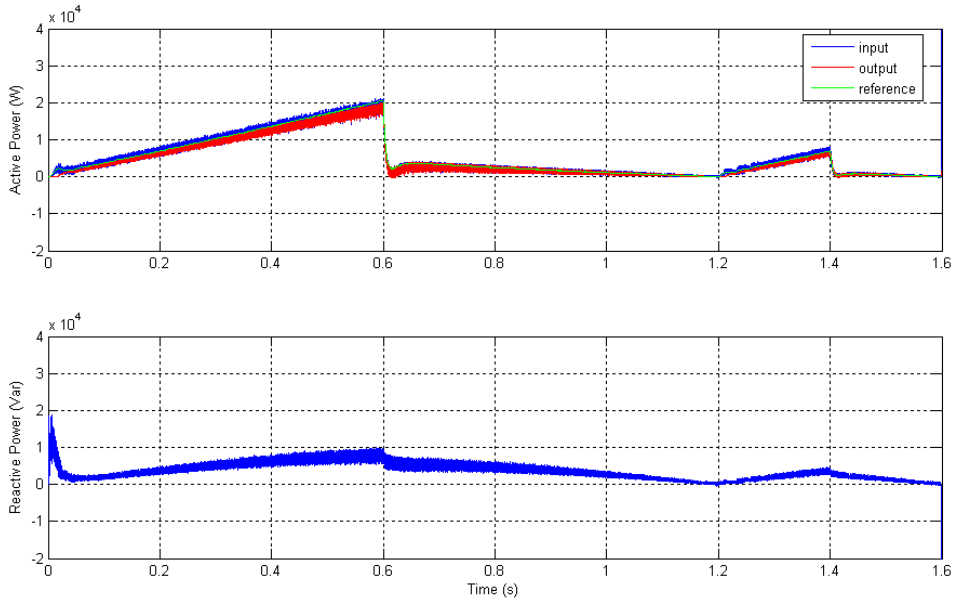

Figure 6.8 Real and reactive power in IM direct input power and flux control: half load.

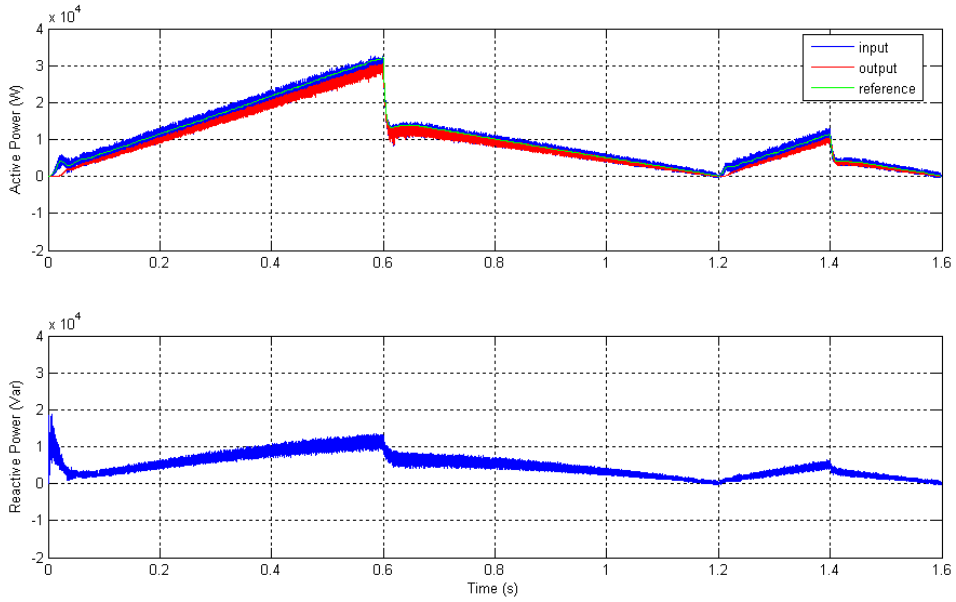

Figure 6.9 Real and reactive power in IM direct input power and flux control: full load.

CHAPER VII

DIRECT REAL POWER AND REACTIVE POWER CONTROL OF INDUCTION MOTORS

When trying to directly control the real and reactive powers of the IM using relay controllers, the major question is how to represent the change of the powers with the change of voltage vectors. The reactive power can be controlled by excitation current, which can be done in synchronous motors, but not in IMs.

7.1 Principles of Control of Real and Reactive Powers

Starting with the equation for apparent power,

$$S_{in} = \frac{2}{3}(\vec{v}_s \vec{i}_s^{\,*}) = P_{in} + jQ_{in} \tag{7.1}$$

substituting the stator current vector as

$$\vec{i}_s = \frac{L_r \vec{\lambda}_s - L_m \vec{\lambda}_r}{L_s L_r - L_m^{\,2}} = \frac{L_r \vec{\lambda}_s - L_m \vec{\lambda}_r}{L_\sigma^{\,2}} \tag{7.2}$$

and employing (6.5), the apparent power can be expressed as

$$S_{in} = \frac{2}{3} j\omega_s \vec{\lambda}_s \left(\frac{L_r \vec{\lambda}_s - L_m \vec{\lambda}_r}{L_\sigma^{\,2}} \right)^*$$

$$= \frac{2}{3} j\omega_s \left(\frac{L_r \vec{\lambda}_s \vec{\lambda}_s^{\,*} - L_m \vec{\lambda}_s \vec{\lambda}_r^{\,*}}{L_\sigma^{\,2}} \right)$$

$$= \frac{2}{3} \frac{\omega_s}{L_\sigma^{\,2}} \left(jL_r \lambda_s^{\,2} - jL_m \vec{\lambda}_s \vec{\lambda}_r^{\,*} \right) \tag{7.3}$$

The real input power is the real part of the apparent power

$$P_{in} = \mathrm{Re}(S_{in}) = \mathrm{Re}\left(\vec{v}_s \vec{i}_s^{\,*}\right)$$

$$= \mathrm{Re}\left[-\frac{2}{3} \frac{\omega_s}{L_\sigma^{\,2}} \left(jL_m \vec{\lambda}_s \vec{\lambda}_r^{\,*} \right) \right]$$

$$= \frac{2}{3} \frac{L_m \omega_s}{L_\sigma^{\,2}} \mathrm{Im}\left(\vec{\lambda}_s \vec{\lambda}_r^{\,*} \right)$$

$$= \frac{2}{3} \frac{L_m \omega_s}{L_\sigma^{\,2}} \lambda_s \lambda_r \sin(\theta_s - \theta_r) \tag{7.4}$$

and the reactive power is the imaginary part of the apparent power

$$Q_{in} = \mathrm{Im}(S_{in}) = \mathrm{Im}\left(\vec{v}_s \vec{i}_s^{\,*}\right)$$

$$= \mathrm{Im}\left[\frac{2}{3} \frac{\omega_s}{L_\sigma^{\,2}} \left(jL_r \lambda_s^{\,2} - jL_m \vec{\lambda}_s \vec{\lambda}_r^{\,*} \right) \right]$$

$$= \frac{2}{3} \frac{\omega_s}{L_\sigma^{\,2}} \mathrm{Re}\left(L_r \lambda_s^{\,2} - L_m \vec{\lambda}_s \vec{\lambda}_r^{\,*} \right)$$

$$= \frac{2}{3} \frac{\omega_s}{L_\sigma^{\,2}} \left[L_r \lambda_s^{\,2} - L_m \, \mathrm{Re}\left(\vec{\lambda}_s \vec{\lambda}_r^{\,*} \right) \right]$$

$$= \frac{2}{3} \frac{\omega_s}{L_\sigma^{\,2}} \left[L_r \lambda_s^{\,2} - L_m \lambda_s \lambda_r \cos(\theta_s - \theta_r) \right] \tag{7.5a}$$

$$= \frac{2}{3} \frac{L_r \omega_s}{L_\sigma^{\,2}} \lambda_s^{\,2} - \frac{2}{3} \frac{L_m \omega_s}{L_\sigma^{\,2}} \lambda_s \lambda_r \cos(\theta_s - \theta_r) \tag{7.5b}$$

7.2 Discussion

The real power in (7.4) is the same as that in (6.1a) and it can be controlled by changing voltage vectors as described in Chapter VI. However, (7.5a) and (7.5b) indicate that the reactive power not only depends on the stator flux but also the stator angular position. The first term can be controlled in the same way as the flux being controlled through voltage vectors, while the presence of the second term means that the problem is more complicated and different from the flux control. In other words, if we use the same principles as for the flux control, we can only control part of the reactive power. The other part will be, in fact, affected by the control of real power because the angle between the two fluxes is changed. The key factor is that this angle difference can be quite large. Therefore, how to control the reactive power is the main issue. Also, the reference for reactive power is difficult to obtain without exact knowledge of motor parameters [6][7].

CHAPER VIII

DIRECT REAL AND REACTIVE POWER CONTROL OF PERMANENT MAGNET SYNCHRONOUS MOTORS

Permanent magnet synchronous motors are different from IMs in the construction and characteristics. However, unlike their sibling BLDCs, they have a sinusoidal back EMF, just as IMs do. Therefore, they can be controlled in a similar way as IMs, for instance, using the FOC and DTC strategies. The question is whether they are suitable for the direct real power and reactive power control.

A general block diagram of direct power control system is shown in Figure 8.1, and a detailed system diagram is presented in Figure 8.2.

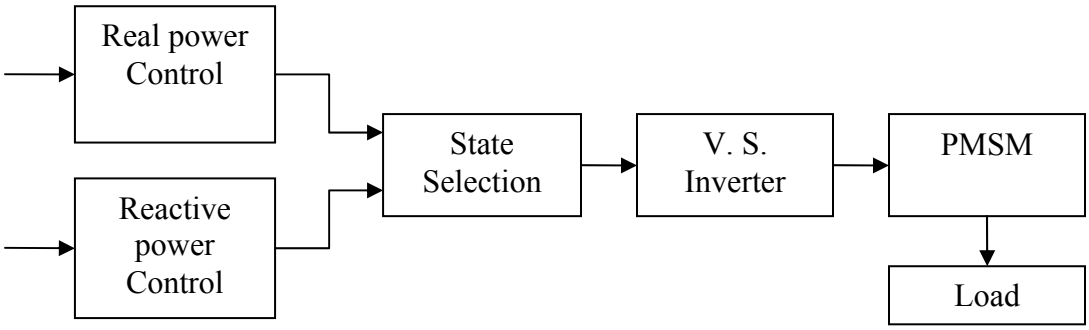

Figure 8.1 A general block diagram of direct power control system for PMSMs.

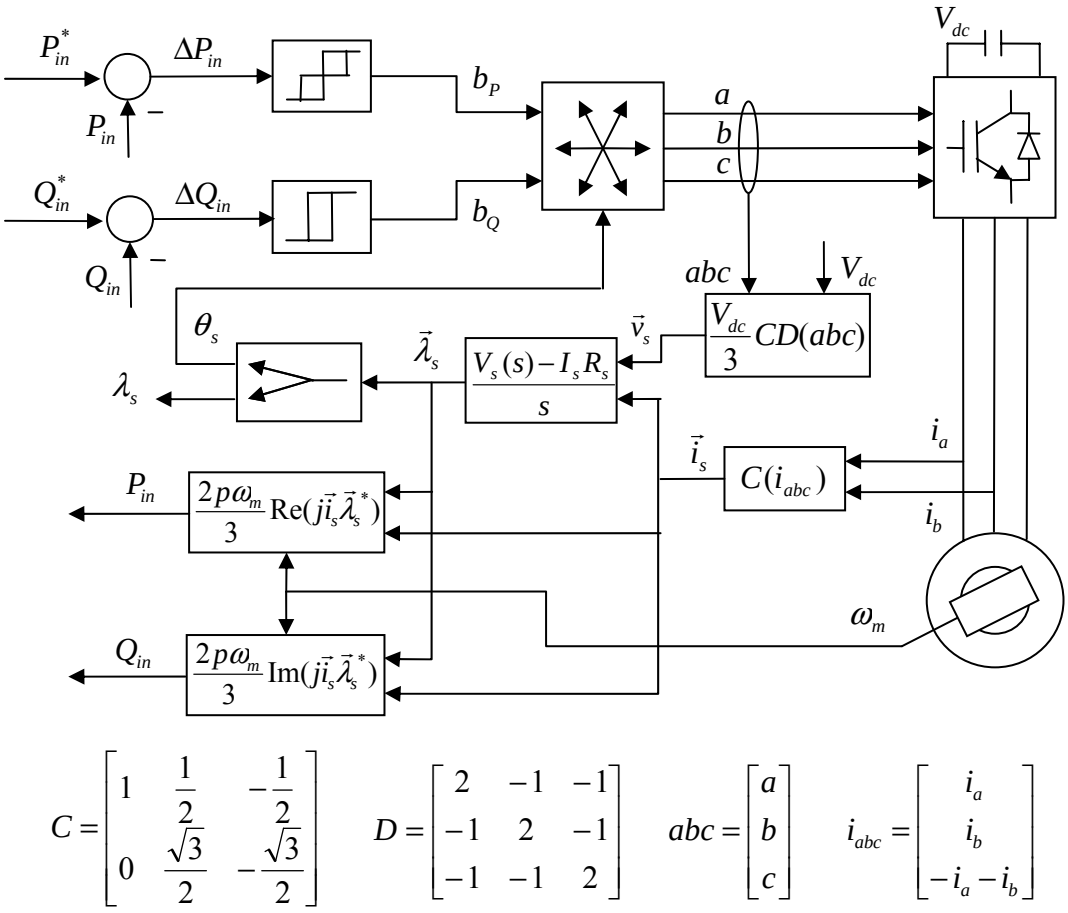

Figure 8.2 The direct real and reactive power control system for PMSMs without a speed loop.

8.1 Principles of Real Power Control

Equation (6.6) for the induction motor is also valid for permanent magnet synchronous motors. Because there is no slip in PMSMs, the input and output real powers are equal when losses are ignored. The real power in the stationary d-q plane can be expressed as

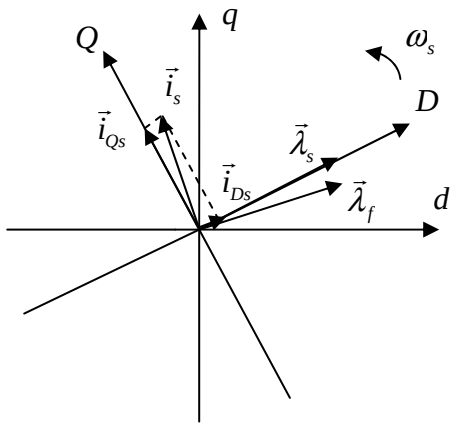

Figure 8.3 Rotating D-Q plane with the stator flux aligned with D axis.

$$P_{in} = \frac{2}{3}\mathrm{Re}(\vec{v}_s \vec{i}_s^{\,*}) = \frac{2\omega_s}{3}(\lambda_{ds} i_{qs} - \lambda_{qs} i_{ds}) \tag{8.1}$$

Employing a rotating D-Q plane, with the stator flux vector aligned with the D axis as illustrated in Figure 8.3, the stator flux can be treated as a DC quantity and the Q axis component becomes zero. Then (8.1) can be rewritten as

$$P_{in} = \frac{2\omega_s}{3}(\lambda_{Ds} i_{Qs}) \tag{8.2}$$

Decomposing (2.24) in D-Q plane, yields

$$\lambda_{Ds} = L_s i_{Ds} + \lambda_{Df} \tag{8.3}$$

$$\lambda_{Qs} = L_s i_{Qs} + \lambda_{Qf} \tag{8.4}$$

and (8.4) can be rearranged to

$$i_{Qs} = \frac{1}{L_s}(\lambda_{Qs} - \lambda_{Qf}) \tag{8.5}$$

Substituting (8.5) in (8.2) allows to express the real power as

$$P_{in} = \frac{2\omega_s}{3L_s}(\lambda_{Ds}\lambda_{Qs} - \lambda_{Ds}\lambda_{Qf}) \tag{8.6}$$

As seen in Figure 8.3, as the rotating D axis is aligned with the stator flux vector, Q axis component of stator flux is zero, and λ_{Ds} is λ_s. Thus,

$$P_{in} = -\frac{2\omega_s}{3L_s}\lambda_s\lambda_{Qf} \tag{8.7}$$

where

$$\lambda_{Qf} = \lambda_f \sin(\theta_r - \theta_s) = -\lambda_f \sin(\theta_s - \theta_r) \tag{8.8}$$

Substituting (8.8) in (8.7) and considering that in PMSMs, $\omega_s = \omega_r$, gives

$$P_{in} = \frac{2\omega_r}{3L_s}\lambda_s\lambda_f \sin(\theta_s - \theta_r) \tag{8.9}$$

Equation (8.9) is similar to (5.2), which indicates that for PMSM motors, the real power can be controlled by increasing or decreasing the stator flux angle using voltage vectors.

8.2 Principles of Reactive Power Control

Similar to the real power case, the reactive power for PMSM is still

$$Q_{in} = \frac{2}{3}\mathrm{Im}(\vec{v}_s\vec{i}_s^{\,*}) = \frac{2\omega_s}{3}(\lambda_{ds}i_{ds} + \lambda_{qs}i_{qs}) \tag{8.10}$$

Converting from the stationary d-q plane to the rotating D-Q plane as shown in Figure 8.3 the reactive power becomes

$$Q_{in} = \frac{2\omega_s}{3}(\lambda_{Ds}i_{Ds}) \tag{8.11}$$

Rearranging (8.3) to

$$i_{Ds} = \frac{1}{L_s}(\lambda_{Ds} - \lambda_{Df}) \tag{8.12}$$

and substituting (8.12) in (8.11), yields

$$Q_{in} = \frac{2\omega_s}{3L_s}(\lambda_{Ds}{}^2 - \lambda_{Ds}\lambda_{Df}) \tag{8.13}$$

From Figure 8.3, it can be seen that λ_{Ds} equals λ_s and

$$\lambda_{Df} = \lambda_f \cos(\theta_r - \theta_s) = \lambda_f \cos(\theta_s - \theta_r) \tag{8.14}$$

Substituting (8.14) in (8.13), and consider that for PMSM motors $\omega_s = \omega_r$, yields

$$Q_{in} = \frac{2\omega_r}{3L_s}[\lambda_s{}^2 - \lambda_s\lambda_f \cos(\theta_s - \theta_r)] \tag{8.15}$$

As the angle between stator flux and permanent magnet flux is small, $\cos(\theta_s - \theta_r) \cong 1$, and (8.15) can be rewritten as

$$Q_{in} \cong \frac{2\omega_r}{3L_s}(\lambda_s{}^2 - \lambda_s\lambda_f) \tag{8.16}$$

Taking the derivative of both sides of (8.16) gives

$$\frac{dQ_{in}}{dt} \cong \frac{2\omega_r}{3L_s}\left(2\frac{d\lambda_s}{dt} - \frac{d\lambda_s}{dt}\lambda_f\right) = \frac{2\omega_r}{3L_s}(2 - \lambda_f)\frac{d\lambda_s}{dt} \tag{8.17}$$

$$\Delta Q_{in} \cong \frac{2\omega_r}{3L_s}(2 - \lambda_f)\Delta\lambda_s \tag{8.18}$$

(8.18) shows that at certain speeds, the change of reactive power is proportional to the change of stator flux. Therefore, the reactive power can be directly controlled by the voltage vectors.

8.3 Real Power Reference

Since there is no slip in operation of PMSM motors, if losses are neglected, the input real power is equal to the output real power. Therefore, the real power reference in a closed-loop control system is the product of the reference speed and reference torque, the latter comes from the output of a classic PI speed controller. Refer to the output power reference section in Chapter IV for details.

8.4 Reactive Power Reference

As described in the output power reference section in Chapter IV, the torque reference can be found at the output of the classic speed controller. And from (2.19), the electromagnetic torque in the stationary d-q reference frame is

$$T_e = \frac{2}{3} p \,\mathrm{Im}(\vec{i}_s \vec{\lambda}_s^{\,*}) = \frac{2}{3} p(\lambda_{ds} i_{qs} - \lambda_{qs} i_{ds}) \tag{8.19}$$

Again, consider the conversion from stationary d-q frame to rotating D-Q frame illustrated in Figure 8.4. Note that this time the D-axis is aligned with the permanent magnet flux λ_f , so that (8.19) can be rewritten in the new frame as

$$T_e = \frac{2}{3} p(\lambda_{Ds} i_{Qs} - \lambda_{Qs} i_{Ds}) \tag{8.20}$$

In order to maximize the torque to current ratio, the stator current should be leading field flux λ_s by a right angle. That is, all stator current is used for magnetization at Q-axis while D-axis current is zero. In practice, this is not possible because there would not be any current to generate reactive power, the motor would not be running. Therefore,

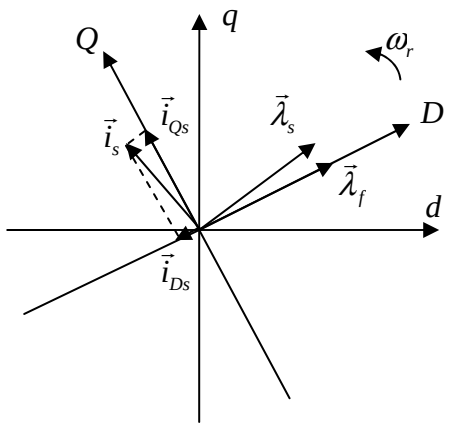

Figure 8.4 Rotating D-Q plane with the rotor PM flux aligned with D axis.

we make the stator current lead permanent magnet flux λ_f by a right angle instead. This causes the angle between stator current and stator flux vectors less than 90º. On the other hand, D-axis stator flux is equal to the permanent magnet flux λ_f . Then (8.20) is reduced to

$$T_e = \frac{2}{3} p \lambda_f i_{Qs} \tag{8.21}$$

By rearranging (8.21), the magnetizing current is obtained as

$$i_{Qs} = \frac{3}{2} \frac{T_e}{p \lambda_f} \tag{8.22}$$

The reactive power in the stationary d-q frame can be expressed as

$$Q_{in} = \frac{2}{3} \omega_r \, \mathrm{Re}(\vec{i}_s \vec{\lambda}_s^{\,*}) = \frac{2}{3} \omega_r (\lambda_{ds} i_{ds} + \lambda_{qs} i_{qs}) \tag{8.23}$$

In the rotating D-Q frame with D axis aligned with the permanent magnet flux λ_f , and the D-axis current of zero, there is

$$Q_{in} = \frac{2}{3}\omega_r \lambda_{Qs} i_{Qs} \tag{8.24}$$

Taking q-axis part of (2.24), and rewriting it in the new D-Q frame yields

$$\lambda_{Qs} = L_s i_{Qs} \tag{8.25}$$

which, when substituted in (8.24), gives

$$Q_{in} = \frac{2}{3}\omega_r L_s {i_{Qs}}^2 \tag{8.26}$$

Finally, when (8.22) is substituted in (8.26), the reactive power can be expressed as

$$Q_{in} = \frac{3}{2}\omega_r L_s \left(\frac{T_e}{p\lambda_f}\right)^2$$

$$= \frac{3}{2p}\omega_m L_s \left(\frac{T_e}{\lambda_f}\right)^2 \tag{8.27a}$$

$$= \frac{3L_s}{2p\omega_m}\left(\frac{P_{in}}{\lambda_f}\right)^2 \tag{8.27b}$$

Either (8.27a) or (8.27b) can be employed as the reactive power reference. The advantage of (8.27b) is that the reactive power is a function of real power. The reactive power reference is obtained whenever the real power reference is known. It is especially valuable when an open-loop power control is applied. Thus, the reactive power reference is given by

$${Q_{in}}^* = \frac{3L_s}{2p\omega_m}\left(\frac{{P_{in}}^*}{\lambda_f}\right)^2 \tag{8.28}$$

Figure 8.5 shows a block diagram realizing (8.28).

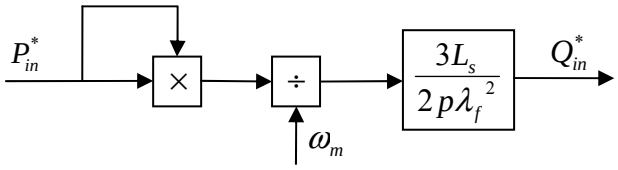

Figure 8.5 Diagram of reactive power reference obtained from real power reference.

8.5 Estimation of the Real and Reactive Powers

Equation (8.1) with $\omega_s = \omega_r$ can be used for estimation of real power:

$$P_{in} = \frac{2\omega_r}{3}(\lambda_{ds} i_{qs} - \lambda_{qs} i_{ds}) = \frac{2p\omega_m}{3}(\lambda_{ds} i_{qs} - \lambda_{qs} i_{ds}) \tag{8.29}$$

while (8.10) with $\omega_s = \omega_r$ can be employed for estimation of reactive power:

$$Q_{in} = \frac{2\omega_r}{3}(\lambda_{ds} i_{ds} + \lambda_{qs} i_{qs}) = \frac{2p\omega_m}{3}(\lambda_{ds} i_{ds} + \lambda_{qs} i_{qs}) \tag{8.30}$$

Figure 8.6 illustrates the described estimation of the real and reactive powers using stator flux and current.

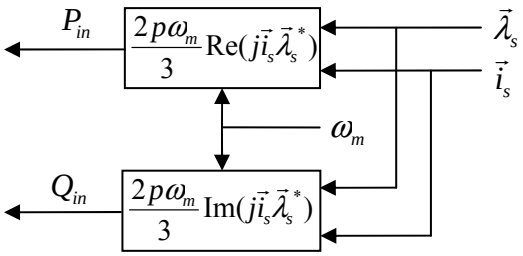

Figure 8.6 Estimation of the real and reactive powers.

8.6 Simulation Results

A MATLAB program was written to simulate the proposed direct power control of PMSMs with a closed-loop speed control. Figure 8.7 shows the system block diagram.

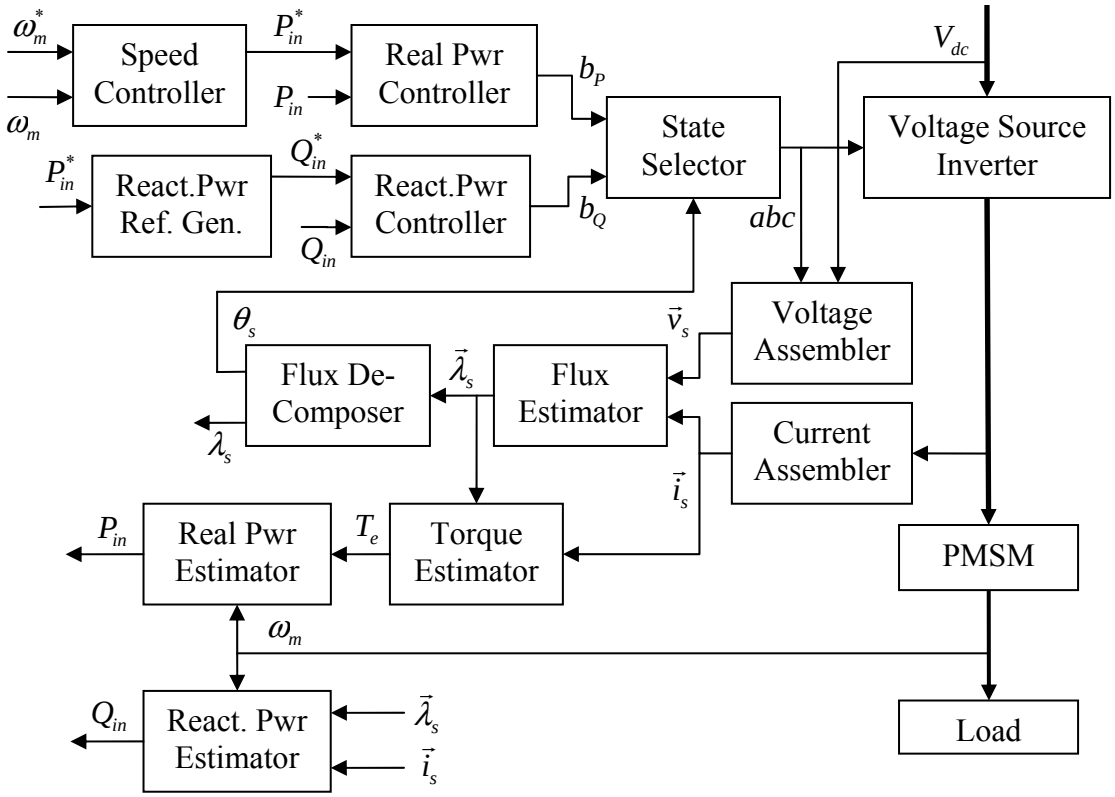

Figure 8.7 Block diagram of the direct power control system for the PMSM with closed-loop speed control

The motor used in simulations is a three-phase 30 hp PMSM, parameters of which can be found in Appendix B. The speed control is the same as that in IM direct power and flux control. The proportional gain K_p and integral gain K_i of the PI controller are the

same 90 and 5000 respectively. The sampling frequency is also 50 kHz. The simulation was run twice, first time with a half load of 55 Nm and second time with a full load of 110 Nm. Threshold for both real and reactive power was 1 W. Relative threshold of 1% was also tested, no obvious difference on the waveforms. For easy comparison, the recorded waveforms of the two different load conditions are placed next to each other. Within each run, the system follows the same speed profile shown in Figures 8.8 and 8.9, which also show the corresponding electromagnetic torque.

It is worth noticing in Figures 8.10 and 8.11, that the current under half load is significantly greater than the current under full load during the time period from 0/8 s to 1.6 s and 1.8 s to 2.0 s. That is due to the negative torque that has been produced in the braking period of the half load situation. The greater current and real power are actually feeding back to the power source. See Figures 8.12 and 8.13 for comparison.

It can be seen in Figures 8.14 and 8.15 that the stator angular position and rotor position of the PMSM are close when load is heavy and almost overlapped when the load is very light. This validates the approximation in (8.16).

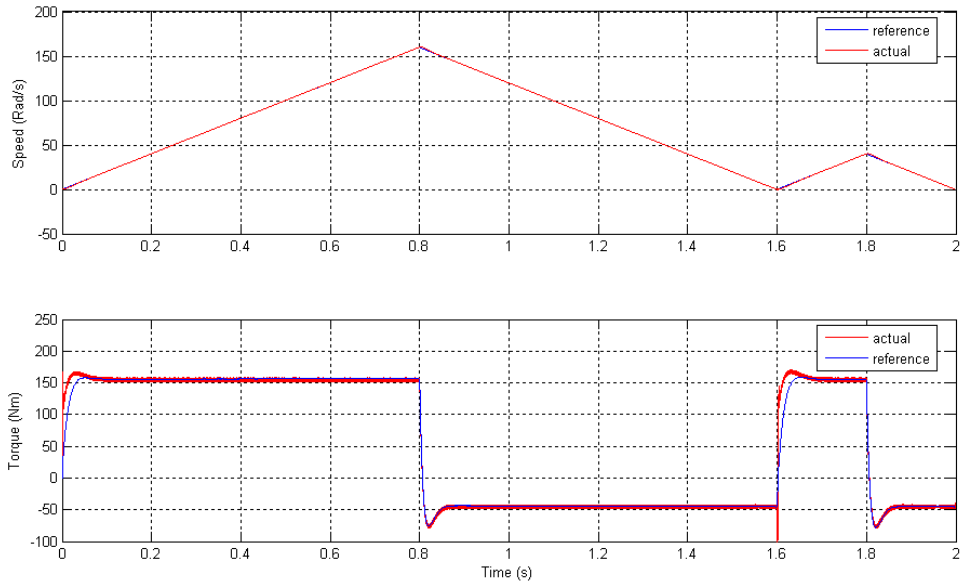

Figure 8.8 Speed and torque in PMSM direct power control: half load.

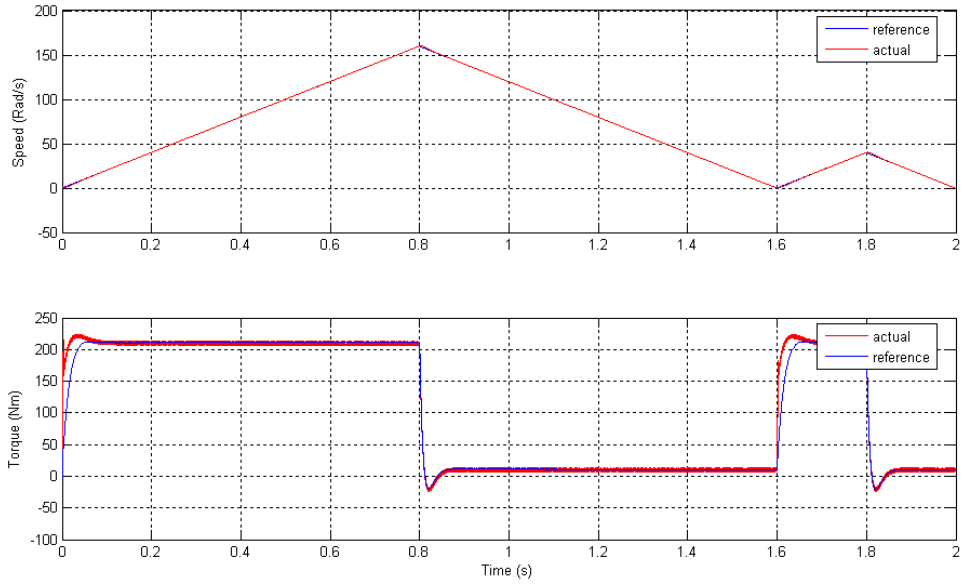

Figure 8.9 Speed and torque in PMSM direct power control: full load.

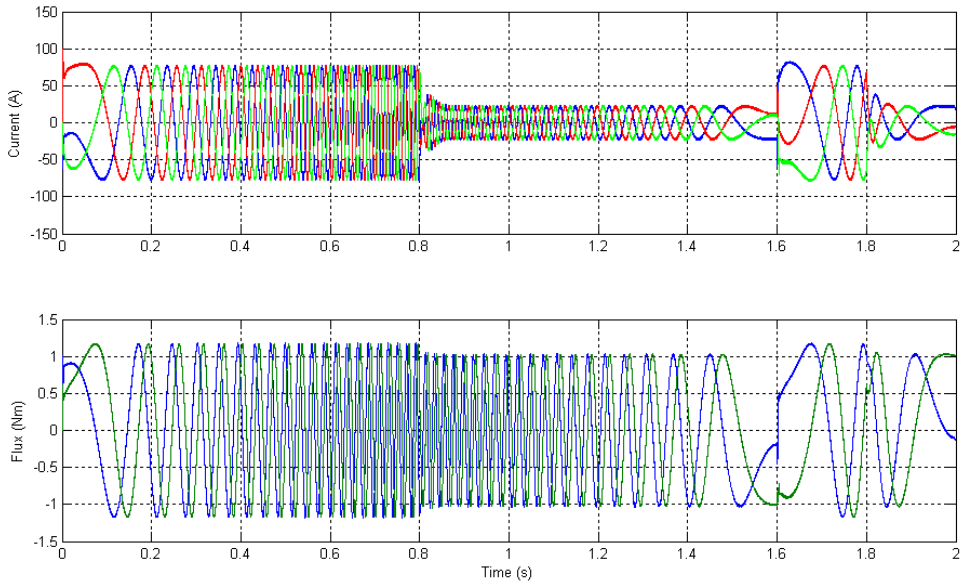

Figure 8.10 Stator current and flux in PMSM direct power control: half load.

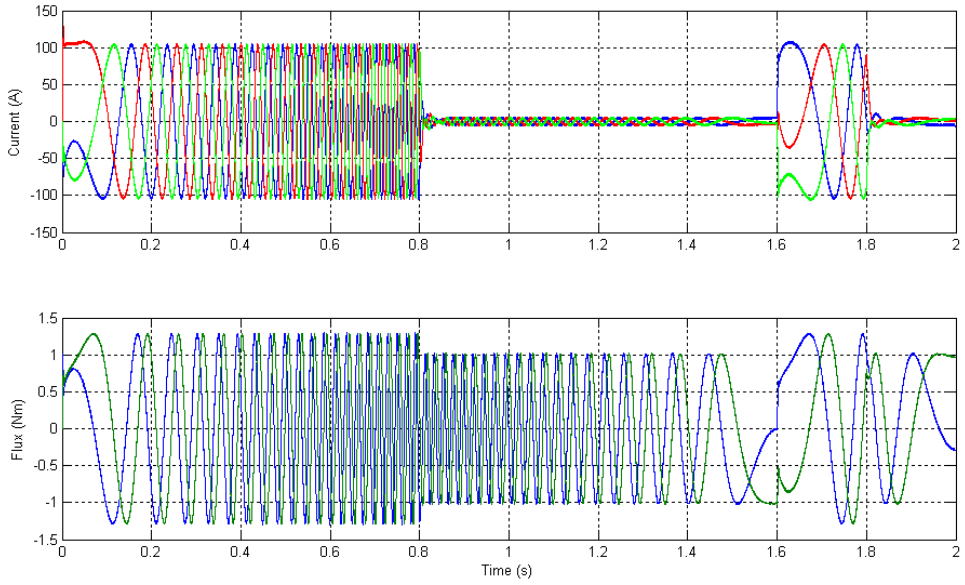

Figure 8.11 Stator current and flux in PMSM direct power control: full load

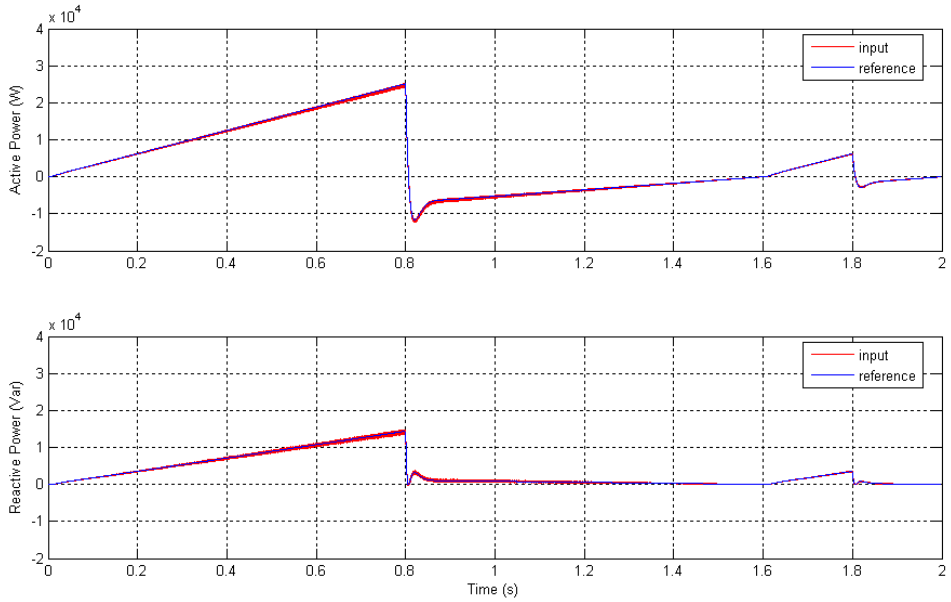

Figure 8.12 Real and reactive powers in PMSM direct power control: half load.

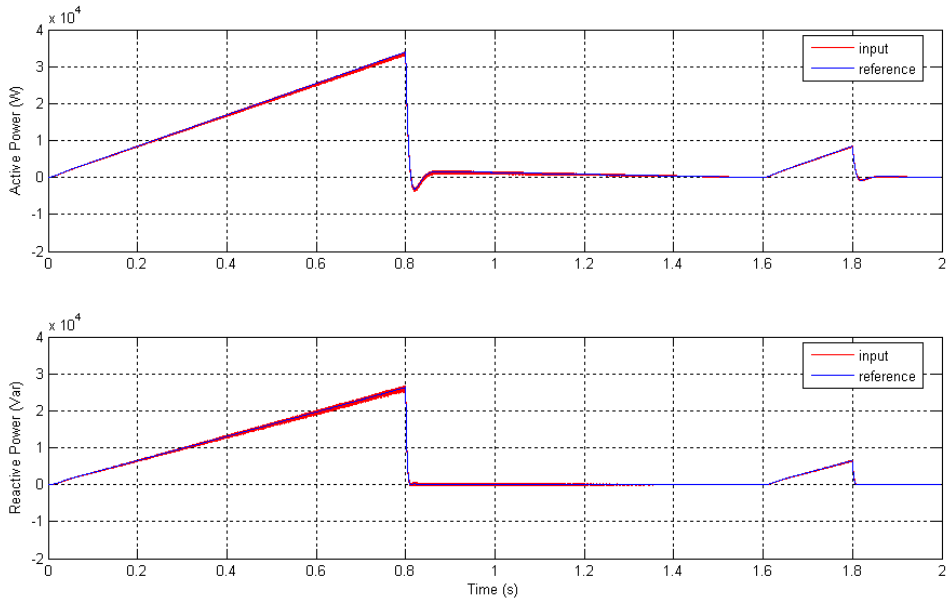

Figure 8.13 Real and reactive powers in PMSM direct power control: full load.

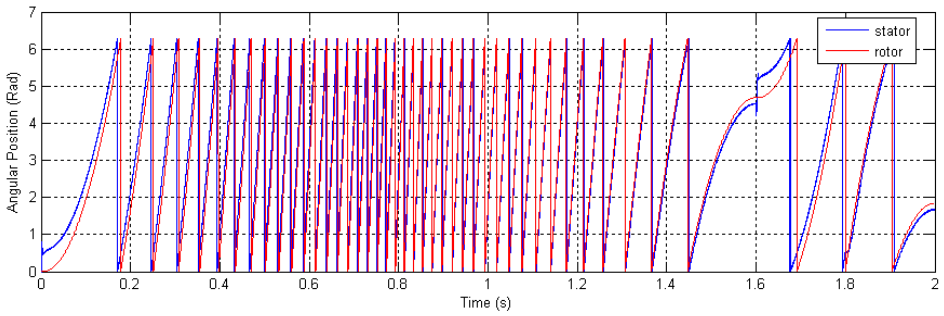

Figure 8.14 Stator and rotor angular position in PMSM direct power control: half load.

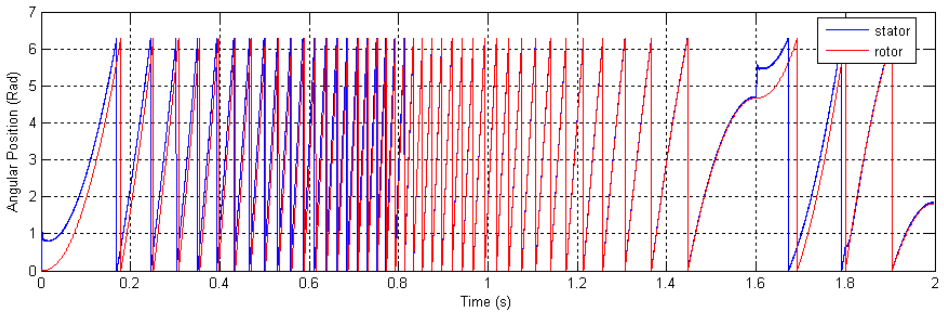

Figure 8.15 Stator and rotor angular position in PMSM direct power control: full load.

CHAPTER IX

CONCLUSION

This thesis described a study of possibilities of direct power control of IMs and PMSMs. Direct output power and flux control, direct input power and flux control approach for IMs, and direct real and reactive power control approach for both the IMs and PMSMs have been proposed and investigated. Simulations using MATLAB have been conducted to evaluate the control methods.

It has been found that the direct output power and flux control, and direct input power and flux control of IMs can be performed, although the performance and stability need further improvements. The simulation results indicate that the output power control performs somewhat better than the input power control in terms of the dynamic response. The system stability in the low motor speed region is better as well. However, the input power control shows a much smoother start, without the high initial spikes of real and reactive power, and electromagnetic torque typical for the starting stage of the output power control.

Simulations were not successful for the direct real and reactive power control of IMs, which is consistent with the theoretical analysis. Without the properly controlled reactive power, the motor does not develop the flux needed for starting. The author believes that poor flux control was the key factor in the simulation failure.

However, the same direct real and reactive power control strategy that has failed with respect to IMs works well with PMSMs. This was validated by both the theoretical analysis and simulation results. The torque is much less rippled than the IM case and the other waveforms are of high quality as well.

REFERENCES

[1] G. Escobar, A. M. Stankovic, J. M. Carrasco, E. Calvan and R. Ortega, "Analysis and design of direct power control (DPC) for a three-phase synchronous rectifier via output regulation subspaces," *IEEE Transactions on Power Electronics*, Vol. 18, No. 3, May 2003.

[2] L. Xu, P. Cartwright, "Direct real and reactive power control of DFIG for wind energy generation," *IEEE Transactions on Energy Conversion*, Vol. 21, No. 3, September 2006.

[3] T. Noguchi, H. Tomiki, S. Kondo and I. Takahashi, "Direct power control of PWM converter without power-source voltage sensors," *IEEE Transactions on Industry Applications*, Vol. 34, No. 3, May/June 1998.

[4] M. Malinowski, M. P. Kazmierkowski, S. Hansen, F. Blaabjerg and G. D. Marque, "Virtual-flux-based direct power control of three-phase PWM rectifiers," *IEEE Transactions on Industry Applications*, Vol. 37, No. 4, July/August 2001.

[5] T. Furuhashi, S. Okuma and Y. Uchikawa, "A study on the theory of instantaneous reactive power," *IEEE Transactions on Industrial Electronics*, Vol. 37, No. 1, February 1990.

[6] R. E. Betz, T. Summers, "Instantaneous power control – an alternative to vector and direct torque control?" in *Proc. IEEE-IAS00*, pp. 1640-1647, 2000.

[7] R. Betz, S. Henriksen, B. Cook, and T. Summers, "Practical aspects of instantaneous power control of induction machines," in Conference Record of the *IEEE-IAS* Annual Meeting, pp. 1771–1778, Oct. 2001.

[8] G. Buja, D. Casadei, and G. Serra, "Direct stator flux and torque control of an IM: Theoretical analysis and experimental results," in *Proc. IEEE-IECON*, Aachen, Germany, 1998, pp. T50–T64.

[9] L. Zhong, M. F. Rahman, W. Y. Hu, and K. W. Lim, "Analysis of direct torque control in permanent magnet synchronous motor drives," *IEEE Transactions on Power Electronics*, Vol 12, No 3, May 1997.

[10] A. M. Trzynadlowski, "Control of Induction Motors," *Academic Press*, 2001.

[11] I. Boldea, S. A. Nasar, "Electric Drives," 2nd Ed., *Taylor & Francis*, 2006.

APPENDIX A

CHARACTERISTICS OF THE EXAMPLE INDUCTION MOTOR

The example motor used in the simulations was a 30 hp three-phase squirrel-cage induction motor. Detailed specifications of the motor are listed in Table A.1 [10].

Table A.1 Parameters of the Example Induction Motor

Parameter	**Symbol**	**Value**
Rated power	P_{rat}	30 hp (22.4 kW)
Rated stator voltage	V_{rat}	230 V/ph
Rated stator current	I_{rat}	39.5 A/ph
Rated frequency	f_{rat}	60 Hz
Rated slip	s_{rat}	0.027
Rated speed	n_{rat}	1168 r/min
Rated torque	$T_{re,at}$	183 Nm
Number of pole pairs	p	3
Stator resistance	R_s	0.294 Ω/ph
Stator inductance	L_s	0.0424 H/ph
Rotor resistance	R_r	0.156 Ω/ph
Rotor inductance	L_r	0.0417 H/ph
Magnetizing inductance	L_m	0.041 H/ph
Rotor mass moment of inertia	J_M	0.4 kg.m^2

APPENDIX B

CHARACTERISTICS OF THE EXAMPLE PERMANENT MAGNET SYNCHRONOUS MOTOR

The example motor used in the simulations was a 30 hp three-phase permanent magnet synchronous motor. Detailed specifications of the motor are listed in Table B.1.

Table B.1 Parameters of the Example Permanent Magnet Synchronous Motor

Parameter	**Symbol**	**Value**
Rated power	P_{rat}	30 hp (22.4 kW)
Rated stator voltage	V_{rat}	230 V/ph
Rated stator current	I_{rat}	39.5 A/ph
Rated frequency	f_{rat}	60 Hz
Rated speed	n_{rat}	1800 r/min
Rated torque	$T_{e,rat}$	118 Nm
Number of pole pairs	p	2
Flux Linkage	λ_f	1.013 Wb
Stator resistance	R_s	0.5 Ω/ph
Stator inductance	L_s	0.005 H/ph
Rotor mass moment of inertia	J_M	0.5 kg.m^2

APPENDIX C

DYNAMIC MODEL OF INDUCTION MOTORS FOR THE SIMULATIONS

The dynamic model described below was used in simulations of the 3-phase squirrel-cage induction motor. The core loss, saturation, slot effects, etc. were neglected. Symbols L_{ls} and L_{lr} denote the stator and rotor leakage inductances, respectively.

$$L_s = L_{ls} + L_m \tag{C.1}$$

$$L_r = L_{lr} + L_m \tag{C.2}$$

The dynamic model of the IM is given in [10] as

$$\frac{d\vec{i}}{dt} = A\vec{v} + B\vec{i} \tag{C.3}$$

where

$$\vec{i} = [i_{ds} \quad i_{qs} \quad i_{dr} \quad i_{qr}]^T \tag{C.4}$$

$$\vec{v} = [v_{ds} \quad v_{qs} \quad v_{dr} \quad v_{qr}]^T \tag{C.5}$$

$$A = \frac{1}{L_\sigma^2}\begin{bmatrix} L_r & 0 & -L_m & 0 \\ 0 & L_r & 0 & -L_m \\ -L_m & 0 & L_s & 0 \\ 0 & -L_m & 0 & L_s \end{bmatrix} \tag{C.6}$$

$$B = \frac{1}{L_\sigma^2}\begin{bmatrix} -R_s L_r & \omega_r {L_m}^2 & R_r L_m & \omega_r L_r L_m \\ -\omega_r {L_m}^2 & -R_s L_r & -\omega_r L_r L_m & R_r L_m \\ R_s L_m & -\omega_r L_s L_m & -R_r L_s & -\omega_r L_s L_r \\ \omega_r L_s L_m & R_s L_m & \omega_r L_s L_r & -R_r L_s \end{bmatrix} \tag{C.7}$$

and

$${L_\sigma}^2 = L_s L_r - {L_m}^2 \tag{C.8}$$

Note that, for induction motor control, this dynamic model was used only in simulations to get more realistic results, the model for theoretical analysis and estimation is given in Chapter II; for the control of permanent magnet synchronous motors, the same model is used in analysis, estimation and simulations, and it is shown in Chapter II.

APPENDIX D

SIMULATION RESULTS OF DIREC TORQUE CONTROL OF INDUCTION MOTORS

For comparison, the simulation results of DTC of induction motors are shown in this appendix. The conditions are all the same as that of DPC of induction motors described in previous chapters, except that the torque control threshold was set at 2 Nm and flux threshold was 0.01 Wb, but relative threshold of 1% rated value also works with a similar result. The rest of this page is left empty so the relevant waveforms can be put next to each other.

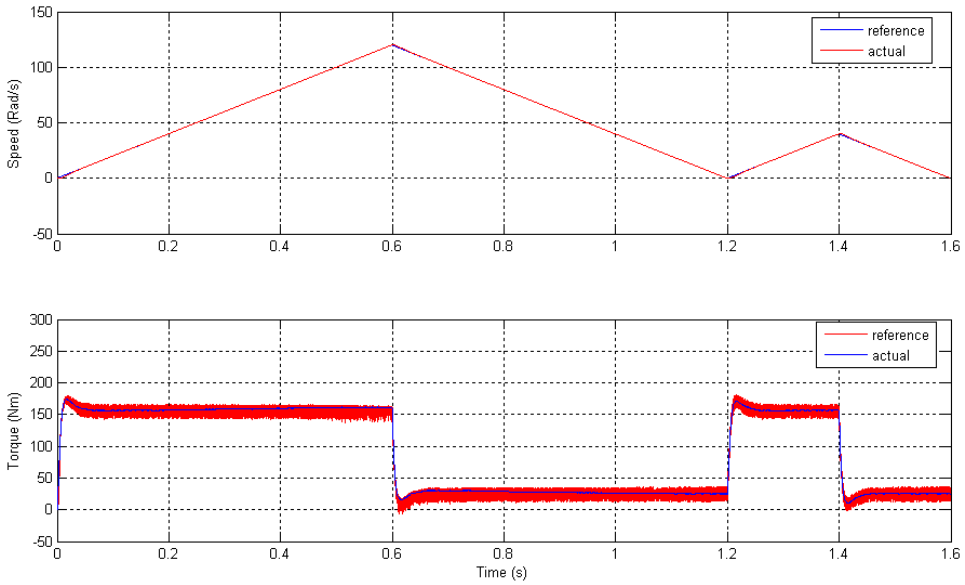

Figure D.1 Speed and torque in IM direct torque control: half load.

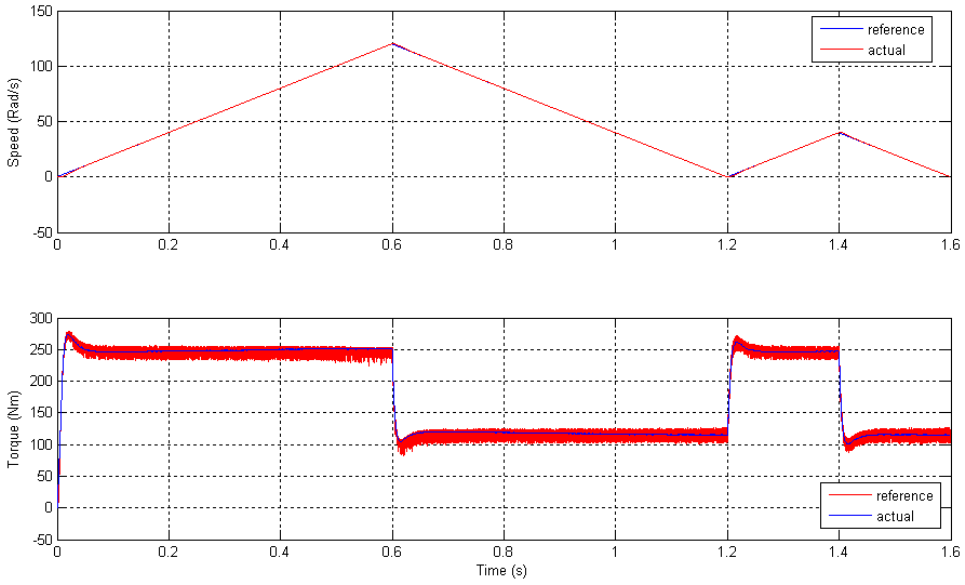

Figure D.2 Speed and torque in IM direct torque control: full load.

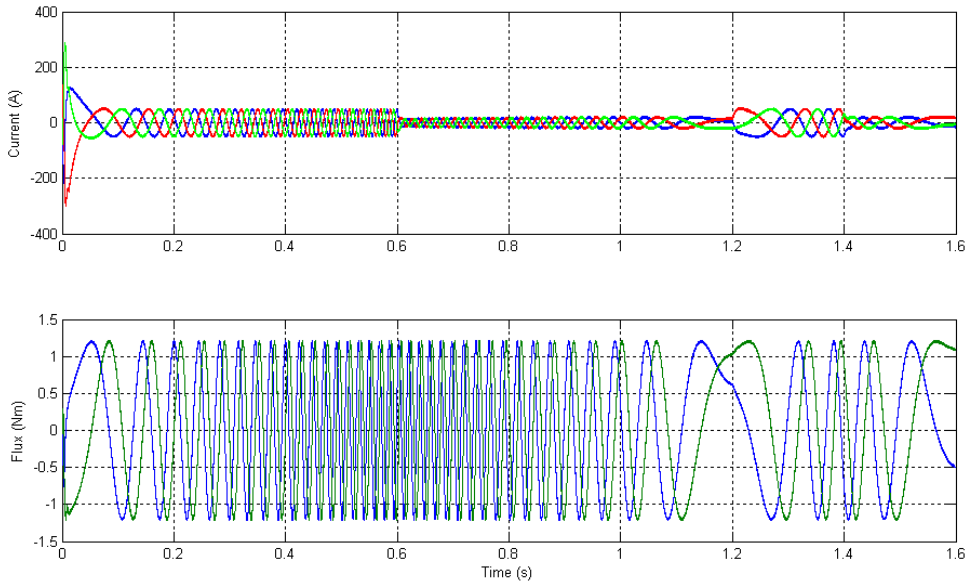

Figure D.3 Stator currents and flux in IM direct torque control: half load.

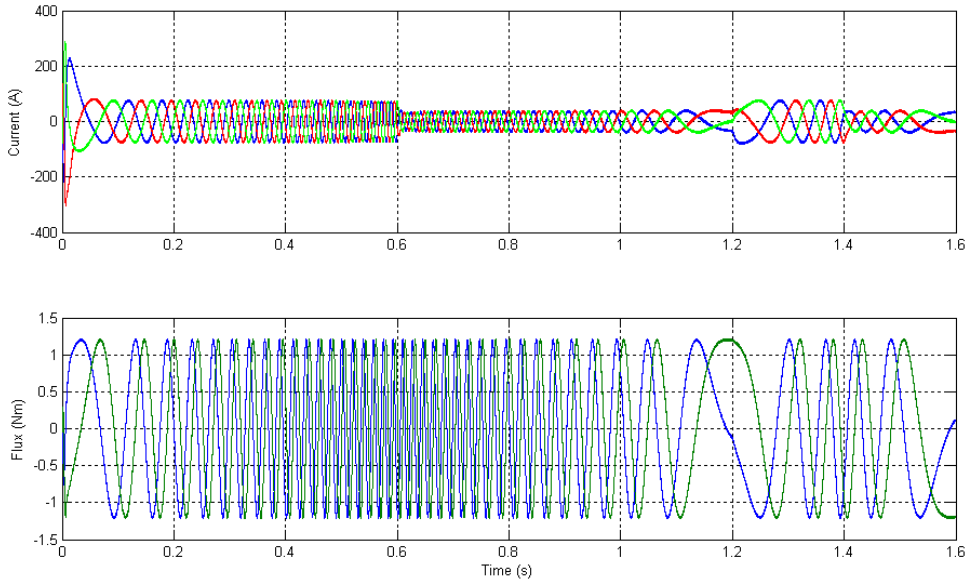

Figure D.4 Stator currents and flux in IM direct torque control: full load.

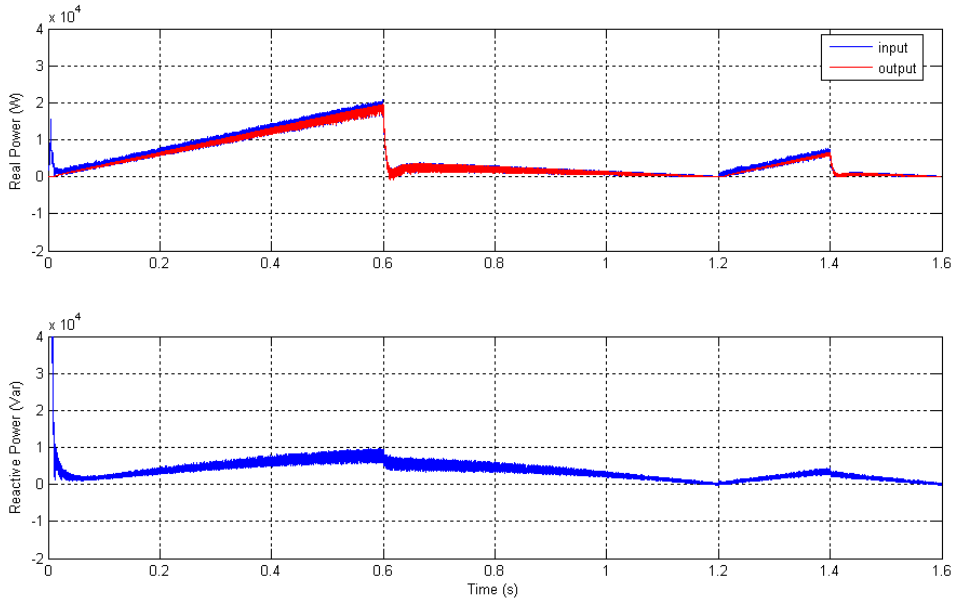

Figure D.5 Real and reactive power in IM direct torque control: half load.

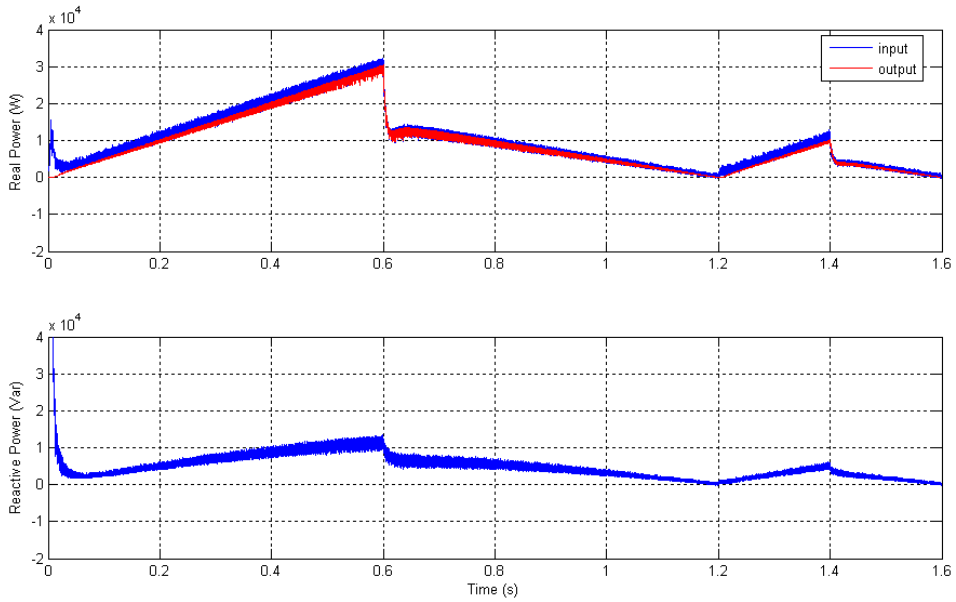

Figure D.6 Real and reactive power in IM direct torque control: full load.